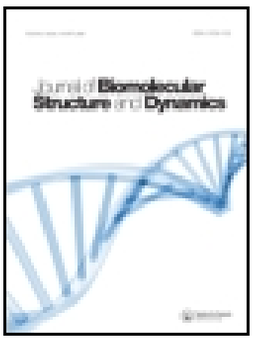

Taylor & Francis
Taylor & Francis Group

Journal of Biomolecular Structure and Dynamics

ISSN: 0739-1102 (Print) 1538-0254 (Online) Journal homepage: http://www.tandfonline.com/loi/tbsd20

Synthesis and preliminary biological evaluation for the anticancer activity of organochalcogen (S/Se) tethered chrysin based organometallic $Ru^{II}(\eta^6$–*p*–cymene) complexes

Shipra Yadav & Jai Deo Singh

To cite this article: Shipra Yadav & Jai Deo Singh (2018): Synthesis and preliminary biological evaluation for the anticancer activity of organochalcogen (S/Se) tethered chrysin based organometallic $Ru^{II}(\eta^6$–*p*–cymene) complexes, Journal of Biomolecular Structure and Dynamics, DOI: 10.1080/07391102.2018.1513867

To link to this article: https://doi.org/10.1080/07391102.2018.1513867

Accepted author version posted online: 20 Aug 2018.

Synthesis and preliminary biological evaluation for the anticancer activity of organochalcogen (S/Se) tethered chrysin based organometallic $Ru^{II}(\eta^6–p–cymene)$ complexes

Shipra Yadav and Jai Deo Singh*

Department of Chemistry, Indian Institute of Technology Delhi (IITD), Hauz Khas, New Delhi 110016, India

*Corresponding author

E–mail: jaideo@chemistry.iitd.ernet.in

Abstract

Organochalcogen (S/Se) functionalized chrysin derivatives were synthesized and coordinated with $Ru^{II}(\eta^6–p–cymene)$ to efficiently form ruthenium based chemotherapeutic drug entities $[C_{31}H_{35}O_4SRuCl]$; $[C_{31}H_{35}O_4SeRuCl]$; $[C_{33}H_{31}O_4SRuCl]$ and $[C_{33}H_{31}O_4SeRuCl]$. The complexes were thoroughly characterized by analytical and various spectroscopic techniques which include elemental analysis, UV–vis, IR, NMR (^1H, ^{13}C and ^{77}Se NMR) and HR–MS. The interaction studies of these Ru(II) complexes were carried out with CT DNA/HSA by employing UV–vis, fluorescence and circular dichroic techniques in view to examine their chemotherapeutic potential. The complexes demonstrated predominant binding towards CTDNA *via* electrostatic interaction while, the extent of binding was quantified by calculating intrinsic binding constant (K_b) and binding constant (K) values which revealed higher binding affinity of selenium based chrysin complexes as compared to their thio–analogs, following the order $[C_{31}H_{35}O_4SeRuCl]$ > $[C_{33}H_{31}O_4SeRuCl]$ > $[C_{31}H_{35}O_4SRuCl]$ > $[C_{33}H_{31}O_4SRuCl]$. Moreover, interaction of these complexes with human serum albumin (HSA) was also investigated which suggested spontaneous interactions of complexes with the protein by hydrogen bonding and van der Waals forces. To visualize the preferential binding sites and affinity of complexes with DNA and HSA molecular docking studies were performed. Additionally, *in vitro* anticancer activity of the complexes were evaluated by SRB assay on selected cancer cell lines *viz.*, HeLa (cervical), MIA–PA–CA–2 (pancreatic), MCF–7 (breast), Hep–G2 (Hepatoma) and SK–OV–3 (ovarian) which exhibited the superior cytotoxicity of complex $[C_{31}H_{35}O_4SeRuCl]$ as compared to other analogs on selective cancer phenotypes.

Keywords: Organochalcogen; $Ru^{II}(\eta^6$–*p*–cymene)complexes; DNA/HSA interaction; *In vitro* Cytotoxicity; Molecular docking.

Abbreviations: Chry, Chrysin; Cym, Cymene; HSA, Human serum albumin; K_b, Binding constant; K_q Quenching constant; K_{sv}, Stern-Volmer constant.

1. Introduction

Platinum based drugs, cisplatin and the follow–on (carboplatin and oxaliplatin) are dominated metallo–chemotherapeutic agents used in a wide number of anticancer treatment regimens (Kelland, 2007). However, their incidences of indiscriminant "off–target" side effects including toxicity and tumor metastasis have limited their effective use as chemotherapeutic agents (Wheate, Walker, Craig and Oun, 2010; Alessio, 2011; Jaouen and Metzler–Nolte, 2010). Consequently, the current cancer treatment scenario demands an urgent and alternative need to develop potential metal complexes that could surmount Pt–based resistances, improve clinical efficacy with reduced toxicity. In this pursuit, Ru(II)–complexes have emerged as a notable class of anticancer drugs because of their favorable kinetic aspects, rich redox chemistry, inherently less toxicity and high selectivity for cancer cells (Allardyce and Dyson, 2001; Clarke, 2003; Hall, Beer, Buchner, Cardin and Cardin, 2015). Significantly, ruthenium complexes might interfere with multiple targets including DNA, proteins and enzymes (Nazarov, Hartinger and Dyson, 2014; Adhireksan et al., 2014; Noffke, Habtemariam, Pizarro and Sadler, 2012,), resulting in comparable or superior cytotoxicity profile against a wide spectrum of cancer phenotypes including the cisplatin–resistant strains (Dyson, 2007) in contrast to Pt–drugs that exhibit cytotoxicity mainly due to covalent interactions with DNA (Reedijk, 1996).

Notably, the success of Ru(III)–complexes **NAMI–A**, [*trans*–$RuCl_4$(1*H*–imidazole) (DMSO–S)], **KP1019**, [*trans*–$RuCl_4$(1*H*–indazole)$_2$] and its Na^+ analogue **NKP1339**, [*trans*–$RuCl_4$(1*H*–indazole)$_2$] in clinical and preclinical trials has led interest in the development of ruthenium based complexes as a new anticancer agents with improved cytotoxicity (Hartinger et al., 2008; Hartinger et al., 2006; Rademaker–Lakhai, Van Den Bongard, Pluim, Beijnen and Schellens, 2004; Weiss et al., 2014). However, in recent years, half–sandwich organoruthenium(II)–arene complexes have exhibited promising *in vivo* antimetastatic, antiangiogenic and anticancer properties (Clavel et al., 2015; Weiss et al., 2015; Berndsen et al., 2017). At the forefront, **RAPTA–C** ($[Ru^{II}(\eta^6$–*p*–cymene)(PTA)$Cl_2]$, PTA = 1,3,5–triaza–7–phosphatricyclo[3.3.1.1]decane), **RAED–C** ($[Ru^{II}(\eta^6$–*p*–cymene)(en)$Cl]^+$) and **RM175**

([Ru^{II}(η^6–biphenyl)(en)Cl], en = ethylenediamine) are the representative examples among this class that are under preclinical trials (Nowak–Sliwinska et al., 2011; Guichard et al., 2006) (**Chart I**).

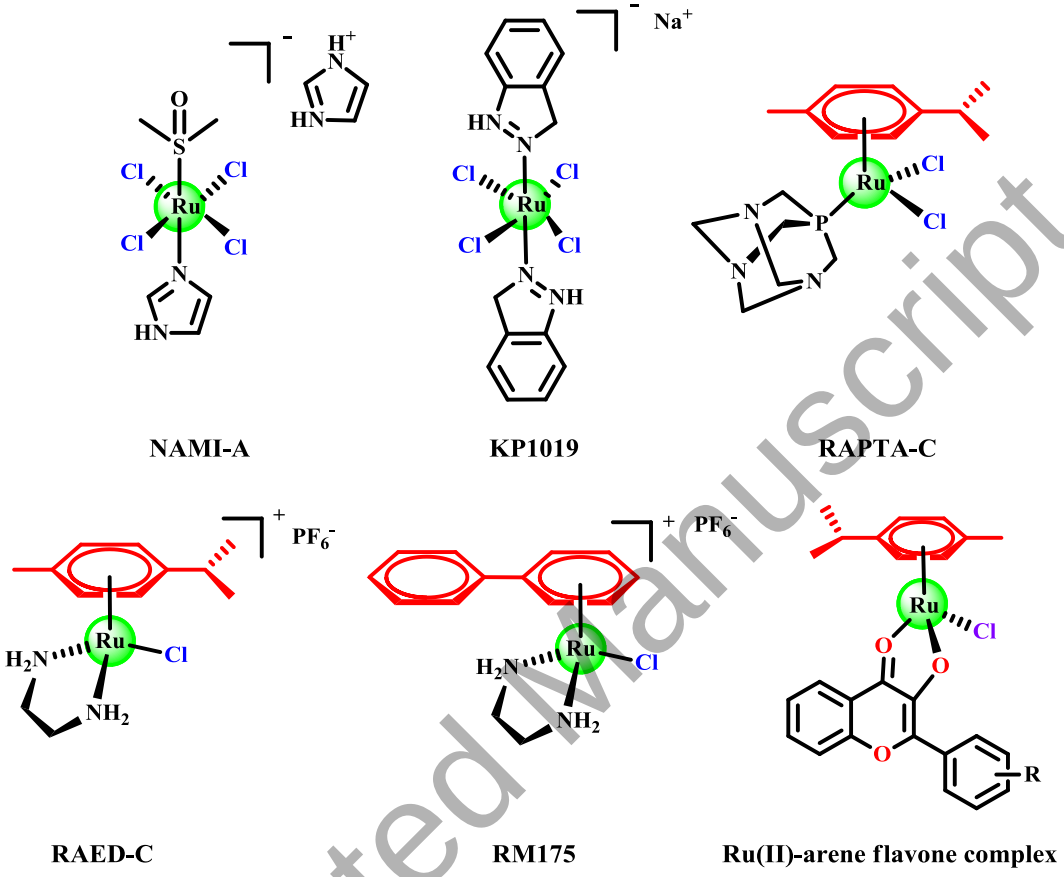

Chart I. Structures of some Ru(II)/(III) promising anticancer agents.

In general, organometallic Ru(II)–arene complexes structurally offer hydrophobic arene group which influences the cellular uptake and kinetic reactivity of Ru(II) complexes (Wang et al., 2005), while the coordinated ligand afford intrinsic control over reactivity and selectivity towards biomolecular targets (Paunescu, McArthur, Soudani, Scopelliti and Dyson, 2016; Riedl et al., 2017) (**Fig. 1**). A wide variety of modifications in Ru(II)–arene complexes have been employed at both the arene moiety and the ancillary mono– or multidentate ligand systems in an effort to precisely tune its anticancer activity. This can be arbitrarily done by inclusion of bioactive organic ligand of known biological functions (Kurzwernhart et al., 2012; Kubanik et al., 2015; Maria et al., 2009).

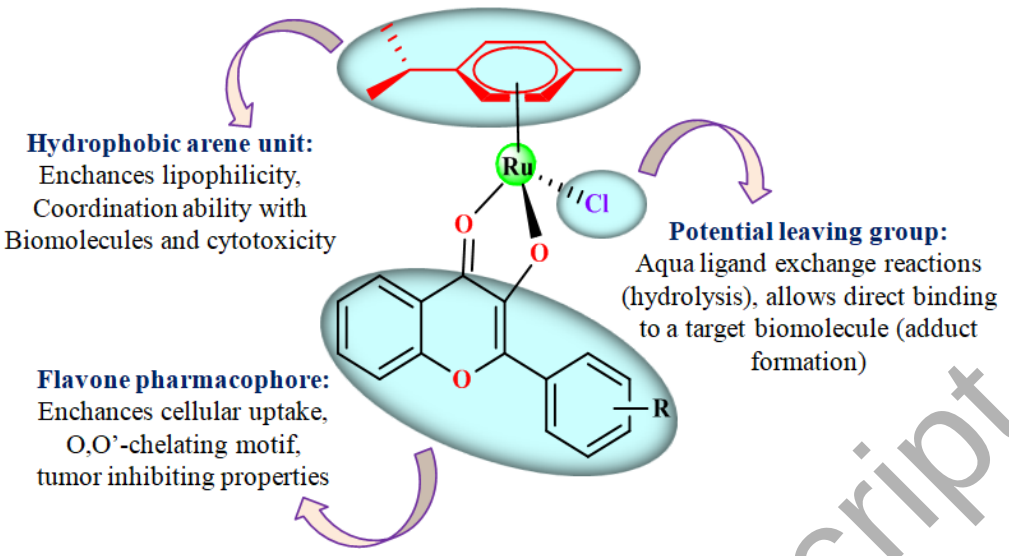

Fig. 1. Graphical scheme showing the general function of different structural elements.

Among them, flavonoids (plant polyphenols) are the most robust and versatile ligands with wide range of pharmaceutical properties *viz*., anti–inflammatory, antimicrobial, antioxidant and anticancer activity (Cushnie, and Lamb, 2005; Middleton, Kandaswami and Theoharides, 2000; Pawara, Tandela, Kunabevub and Jaldappagari, 2018). In particular, chrysin is a natural flavone that has shown to induce growth inhibition and apoptosis in multiple cancer cell lines (Yang et al., 2014; Pichichero, Cicconi, Mattei and Canini, 2011). Chrysin is an efficient chemopreventive agent (Rehman et al., 2013) that offer 3–hydroxy–4–keto system as a *O,O'*–chelating motif for $Ru^{II}(\eta^6$–*p*–cymene) moiety which not only augment the bioavailability and multitargeted approach but also synergizes it to act in concord at the target site (Grazul and Budzisz, 2009; Kurzwernhart et al., 2012). Recently, reports have revealed that functionalization of chrysin scaffold improves its aqueous solubility, protein interactions and cytotoxic activity (Singh, Kaur and Silakari, 2014; Kurzwernhart et al., 2013).

Our interest stems in modulating the chrysin unit by incorporation of organochalcogen moiety with Ru(II) metal centre which could synergize the effects of these artifacts by specifically enhancing the selectivity towards biomolecules. Sulfur (S) and selenium (Se) containing derivatives exhibit prevention against cancer mainly due to their functions in radical scavenging and enzymatic decomposition of oxygen metabolites (Battin and Brumaghim, 2009). Indeed, selenium is recognized as an essential micronutrient of particular interest owing to its ability to participate in crucial redox reactions particularly implicated in antioxidant (Rahmanto and

Davies, 2012), chemopreventive (Janakiram et al., 2013) or apoptotic activities (Sanmartín, Plano and Palop, 2008). Additionally, it has been suggested that mechanisms of action by which seleno– complexes exert their anticancer acitivity includes induction of apoptosis, inhibition of angiogenesis and modulation of AKT and COX pathway (Sanmartin, Plano, Sharma & Palop, 2012). In fact, incorporation of selenium in bioactive ligand is a successful strategy that exhibited synergistic effects to chemotherapeutic drugs (Martins et al., 2013; Qi et al., 2012) leading to inhibition of cancer cell growth in various xenograft of rat models for different cancer phenotypes (Zeng, Cheng and Johnson, 2013; Nguyen et al., 2011).

Herein, we report synthesis and characterization of new organometallic Ru(II) complexes [$C_{31}H_{35}O_4SRuCl$], **1**; [$C_{31}H_{35}O_4SeRuCl$], **2**; [$C_{33}H_{31}O_4SRuCl$], **3**; and [$C_{33}H_{31}O_4SeRuCl$], **4** from chrysin derivatives (**L_1–L_4**) with the general formula (RE–chry) {where, RE = ^{n}BuS (**L_1**); ^{n}BuSe (**L_2**); PhS (**L_3**) and PhSe (**L_4**)}. We have further carried out interaction studies of these complexes by various spectroscopic studies in order to validate their chemotherapeutic candidature. The complexes were screened for their cytotoxicity by SRB assay against different cancer cell lines which revealed the superior cytotoxicity of complex **2** as compared to other analogs on selective cancer phenotypes. Therefore, the key strategy of our current study provide an important rationale for the design of new Ru(II) metallodrugs towards exploring the important modulation in their chemotherapeutic candidature by tethering organochalcogen motif at bioactive chrysin unit.

2. Experimental section

2.1. Materials

All chemicals *viz.*, bis[(η^6–*p*–cymene)dichloridoruthenium(II)], chrysin (TCI, India), 1,2–dibromoethane, 1–bromobutane, bromophenyl (Spectrochem), K_2CO_3 (Fisher scientific), selenium(CDH), *n*–butanethiol, sodium methoxide, thiophenol (Aldrich), and tris(hydroxymethyl)aminomethane or tris buffer (Fisher scientific) were of AR grade and used as received. Disodium salt of calf–thymus DNA (CT DNA) and human serum albumin (HSA) with a molecular mass of 66478 Da were purchased from Sigma Aldrich and stored at 4 ºC. 7–(2–Butylthio)ethoxy)–5–hydroxy–2–phenyl–4*H*–chromen–4–one (**L_1**), 7–(2–butylselanyl)ethoxy)–5–hydroxy–2–phenyl–4*H*–chromen–4–one (**L_2**), 5–hydroxy–2–phenyl–7–(2–phenylthio)ethoxy)–4*H*–chromen–4–one (**L_3**) and 5–hydroxy–2–phenyl–7–(2–phenylselanyl)ethoxy)–4*H*–chromen–4–one (**L_4**) were synthesized according to previously

reported procedures with slight modification (Lee,Park, Kim, Jung and Cho, 1995; Fonseca et al., 2015). All the reactions were carried out in anhydrous conditions using dry solvents under inert atmosphere.

2.2. Instrumental methods

Elemental analyses (C, H and N) were performed on Perkin Elmer series II 2400 CHNO Rapid elemental analyzer. IR spectra for all derivatives were recorded from KBr pellets in the range 4000–400 cm^{-1} using Nicolet, Protege 460 FT–IR spectrometer. ^{1}H and ^{13}C NMR spectra were recorded on a Bruker Spectrospin DPX–300 spectrometeroperating at 300.13 and 75.46 MHz, respectively using $CDCl_3$ as a solvent and tetramethylsilane (TMS) as internal standard, while ^{77}Se NMR spectra were carried on Bruker–400 operating at 76.31 MHz in $CDCl_3$ solvent. High resolution mass spectra (HR–MS) were obtained on Bruker MS–632 mass spectrometer. Samples were prepared at μM level in CH_3CN solvent. UV–vis spectra were recorded at room temperature on a Perkin–Elmer Lambda 35 spectrometer against a solvent blank reference in the wavelength range of 250–650 nm. Fluorescence measurements were carried out on a HORIBA–Jobin Yvon Scientific Fluoromax–4 equipped with quartz cells (1.0 cm), setting the widths of both excitation and emission slits to 5 nm. CD spectra were measured on Jasco J–815–CD spectropolarimeter (Jasco, Japan) at room temperature using a 1 cm quartz cuvette.

2.3. DNA Interaction Studies

2.3.1. UV–vis absorption studies

DNA concentration was determined spectrophotometrically by assuming ε_{260nm} = 6600 $M^{-1}cm^{-1}$ (Marmur, 1961). The absorption titration of complexes in Tris–HCl buffer were performed by using a fixed concentration of Ru(II) complexes (0.2 x 10^{-6} M) with increasing concentration of CT DNA (0.1–1.0 x10^{-6} M).The intrinsic binding constant, K_b value of the complex to CT DNA was determined by Wolfe–Shimer equation (1) (Wolfe, Shimer and Meehan, 1987).

$$\frac{[DNA]}{\varepsilon_a - \varepsilon_f} = \frac{[DNA]}{\varepsilon_b - \varepsilon_f} + \frac{1}{K_b(\varepsilon_a - \varepsilon_f)} \qquad (1)$$

where [DNA] represents the concentration of DNA and ε_a, ε_f, ε_b, the apparent extinction coefficient (A_{obs}/[M]), the extinction coefficient for free metal complex (M), and the extinction coefficient for the complex (M) in the fully bound form, respectively. The slope and intercept of the linear fit of the plot of [DNA]/|ε_a–ε_f| *vs.* [DNA], give 1/|ε_a–ε_f| and 1/K_b|ε_a–ε_f|, respectively. The intrinsic binding constant, K_b can be obtained from the ration of the slope to the intercept.

2.3.2. Fluorescence spectral studies

Relative binding of Ru(II) complexes with CT DNA was studied by fluorescence spectral method using CT DNA solution in Tris–HCl buffer (pH 7.2). In an experiment, complex solution (0.2 x10^{-6} M) was added to the increasing concentrations of CT DNA (0–1.2 x 10^{-6} M). The fluorescence intensity measured at excitation wavelength 270 nm in the range of 310–500 nm. Binding constant, *K* of the metal complexes was determined using following Scatchard equation (2 & 3) by emission titration (Cui et al., 2009).

$$C_F = C_T (I/I_o – P) (1 – P) \quad (2)$$

$$r/C_F = K (n – r) \quad (3)$$

where, C_F is the free metal complex concentration, C_T is the total concentration of the probe added, I and I_o are fluorescence intensities in presence and absence of CT DNA, respectively and P is the ratio of the observed fluorescence quantum yield of bound probe to that of the free probe. The value P was obtained as the intercept by extrapolating from a plot of I_o/I *vs.* 1/[DNA], r denotes ratio of C_B ($C_B = C_T – C_F$) to the DNA concentration i.e., the bound probe concentration to the CT DNA concentration, K is the binding constant and *n* is the number of binding sites.

2.4. HSA Interaction Studies

2.4.1. UV–vis absorption studies

The stock solutions of HSA were prepared by dissolving the solid HSA in 50 mM Tis–HCl, 100 mM NaCl buffer at pH 7.2. HSA concentration was determined from absorption spectra, using the value of ε_{278nm} = 36000 M^{-1} cm^{-1} (Samari, Hemmateenejad , Shamsipur, Rashidi and Samouei, 2012) and absorbance of a 1 mg ml^{-1} solution at ~280 nm (λ_{max} Trp–214).The absorption titrationof complexes in Tris–HCl buffer (pH 7.2) were performed by using a fixed concentration of HSA (2.0 x 10^{-6} M) with increasing concentration of complexes (0–4.0 x 10^{-6} M). The value of binding constants can be calculated from the double reciprocal plot of $1/A – A_o$ *vs.* $1/C_{complex}$ by using the following equation (4) (Stephanos, 1996):

$$\frac{A_o}{A - A_o} = \frac{\varepsilon_{HSA}}{\varepsilon_B} + \frac{\varepsilon_{HSA}}{\varepsilon_B K} \frac{1}{C_{Complex}} \quad (4)$$

Where A_o and A are the absorbance of HSA at ~280 nm, in the absence and presence of complex, respectively. ε_{HSA} and ε_B are the molar extinction coefficient of HSA and the bound complex, respectively, and *l* is the light path of the cuvette (1 cm).

2.4.2. Fluorescence spectral studies

Fluorescence measurements were carried with the excitation and emission wavelength set at 290 and 300–500 nm, respectively. For fluorescence measurements, fixed concentration of HSA (1.0 x 10^{-6} M) was titrated with varying concentrations (0–4.0 x 10^{-6} M) of complexes at 300 and 310 K. The intensity at 350 nm (Tryptophan) was used to calculate the binding constant, K. The fluorescence quenching of HSA at different temperatures (300 and 310 K) were determined using the Stern–Volmer equation (Soares, Mateus and de Freitas, 2007):

$$\frac{F_o}{F} = 1 + K_q \tau_o [Q] = 1 + K_{SV} [Q] \quad (5)$$

where F_o and F are the fluorescence intensities in absence and presence of quencher, respectively, [Q] is the quencher concentration, and K_{sv} is the Stern–Volmer quenching constant, K_q is the biomolecular quenching rate constant and τ_o is the average lifetime of the fluorophore in absence of quencher and its value is around 10^{-8} s for most biomolecules. K_{sv}values were calculated from F_o/F *vs.* [Q] plot, whereas from the log (F_o/F–1) *vs.* log [Q] plot, the number of binding sites (*n*) and the binding constants (K) were calculated.

2.4.3. Determination of thermodynamic parameters

The thermodynamic parameters were calculated from the van′t Hoff equation (Cheng, Fang, Bai, Ouyang and Hu, 2017):

$$\ln K = \frac{-\Delta H}{RT} + \frac{\Delta S}{R} \quad (6)$$

where *K* is the Lineweaver–Burk static quenching constant at corresponding temperature and R is the gas constant, in which ΔH and ΔS of reaction was determined from the linear relationship between ln K and the reciprocal absolute temperature. Furthermore, the free energy change (Δ*G*) was calculated by the equation:

$$\Delta G = \Delta H - T\Delta S = -RT \ln K \quad (7)$$

2.4.4. Three–dimensional (3D) fluorescence spectral studies

Three–dimensional fluorescence spectroscopy is a method for providing conformational and structural information of proteins. The maximum emission wavelength and the fluorescence intensity of the residues have a close relation to the polarity of their micro–environment. The excitation and emission slits were set at 5 nm andrespective blanks were sbstracted.

2.4.5. CD spectral studies

The CD spectra of DNA were collected in the presence of **1–4** at molar ratio of 1:1 in the range of 200–250 nm, with 20 nm/min scan speed and a response time of 2s. Similarly, the CD spectra of HSA were collected in the presence of complexes at molar ratio of 1:1 in the range of 200–250 nm. Measurements were taken at wavelengths between 200 and 250 nm.

2.5. Molecular docking studies

The rigid molecular docking studies were performed by using HEX 6.3 software, which is an interactive molecular graphics program for the interaction, docking calculations, and to identify possible binding site of the biomolecules (Mustard and Ritchie, 2005). Structures of the complexes were sketched by CHEMSKETCH (http://www.acdlabs.com) and converted to pdb format. The crystal structure of the B–DNA (PDB ID: 1BNA) and HSA (PDB ID: 1h9z) were retrieved from the protein data bank (http://www.rcsb.org./pdb). Visualization of the docked pose has been performed by using Pymol and Discovery Studio 3.5 softwares.

2.6. In vitro antitumor studies

The cell lines used for *in vitro* antitumor activity were HeLa (cervical), MIA–PA–CA–2 (pancreatic), MCF–7 (breast), Hep–G2 (Hepatoma), SK–OV–3 (ovarian). The cell lines were grown in RPMI 1640 medium containing 10% fetal bovine serum and 2 mM L–glutamine. For present screening experiment, cells were inoculated into 96 well microtiter plates in 90 µL at 5000 cells per well. After cell inoculation, the microtiter plates were incubated at 37 °C, 5% CO_2, 95% air and 100% relative humidity for 24 h prior to addition of experimental drugs. Experimental drugs were solubilized in appropriate solvent to prepare stock of 10^{-2}M concentration. At the time of experiment four 10–fold serial dilutions were made using complete medium. Aliquots of 10 µl of these different drug dilutions were added to the appropriate micro–titer wells already containing 90 µl of medium, resulting in the required final drug concentrations. After compound addition, plates were incubated at standard conditions for 48 hours and assay was terminated by the addition of cold TCA. Cells were fixed *in situ* by the gentle addition of 50 µl of cold 30 % (w/v) TCA (final concentration, 10 % TCA) and incubated for 60 minutes at 4°C. The supernatant was discarded; the plates were washed five times with tap water and air dried. Sulforhodamine B (SRB) solution (50 µl) at 0.4 % (w/v) in 1 % acetic acid was added to each of the wells, and plates were incubated for 20 minutes at room temperature. After staining, unbound dye was recovered and the residual dye was removed by washing five

times with 1 % acetic acid. The plates were air dried. Bound stain was subsequently eluted with 10 mM trizma base, and the absorbance was read on an Elisa plate reader at a wavelength of 540 nm with 690 nm reference wavelength. Percent growth was calculated on a plate–by–plate basis for test wells relative to control wells and was expressed as the ratio of average absorbance of the test well to the average absorbance of the control wells*100. Using the six absorbance measurements [time zero (T_z), control growth (C), and test growth in the presence of drug at the four concentration levels (T_i)], the percentage growth was calculated at each of the drug concentration levels. The dose response parameters were calculated for each test article. Growth inhibition of 50 % (GI_{50}) was calculated from $[(T_i–T_z)/(C–T_z)] \times 100 = 50$, which is the drug concentration resulting in a 50% reduction in the net protein increase (as measured by SRB staining) in control cells during the drug incubation. The drug concentration resulting in total growth inhibition (TGI) was calculated from $T_i = T_z$. The LC_{50} (concentration of drug resulting in a 50% reduction in the measured protein at the end of the drug treatment as compared to that at the beginning) indicating a net loss of cells following treatment is calculated from $[(T_i–T_z)/T_z] \times 100 = –50$.

3. Results and discussion

Organochalcogen (S/Se) functionalized chrysin ligands **L_1–L_4** and their corresponding $Ru^{II}(\eta^6$–*p*–cymene) complexes **1–4** were synthesized and characterized by various spectroscopic methods. The synthetic route for organochalcogen derivatives of chrysin ligands involved the preparation of bromo–chrysin intermediate, **L** (Hu, Wang, Cheng, Pan and Ren, 2011). The bromo–chrysin ligand, **L** was obtained by reacting chrysin with 1,2–dibromoethane in the presence of K_2CO_3 as a base and acetone as solvent. Both sulphur and selenium functionalized chrysin ligands, **L_1–L_4** were synthesized by reacting bromo–chrysin (**L**) with different organochalcogenolate anions (**Scheme I**). In case of thio–functionalized chrysin ligands **L_1** &**L_3**, thiolate anions were generated *via* reaction of respective thiols with sodium under a nitrogen atmosphere, while seleno–tethered ligands **L_2** & **L_4**, were obtained from organoselenolate anions generated *in situ* from the respective diorganyl diselenide in the presence of sodium borohydride.

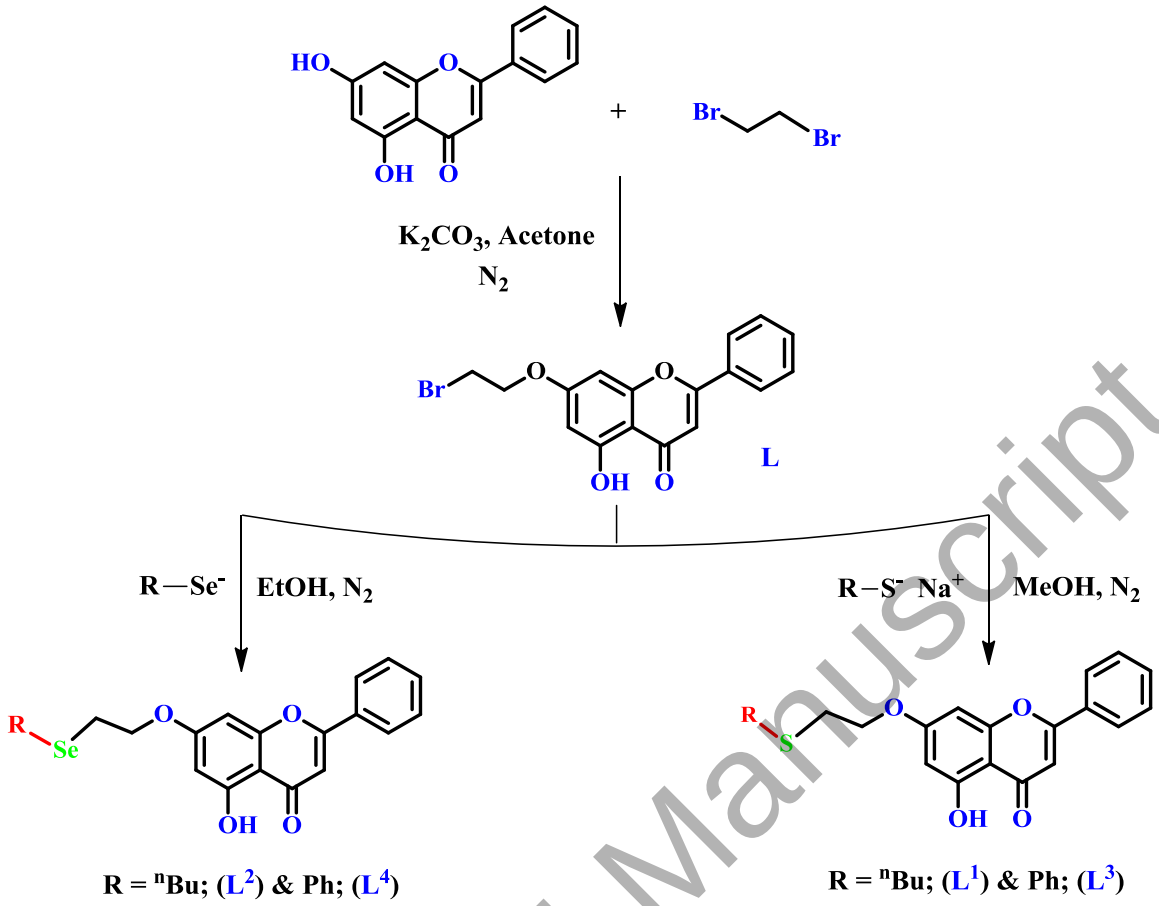

Scheme I. Synthetic route of modified chrysin ligands, $\mathbf{L_1}$–$\mathbf{L_4}$.

Organoruthenium(II)–arene complexes **1–4** were synthesized by reacting ligands $\mathbf{L_1}$–$\mathbf{L_4}$ with $[Ru(\eta^6\text{–}p\text{–cymene})Cl_2]_2$ salt in presence of NaOMe (used for deprotonation of the hydroxyl group of chrysin moiety) (**Scheme II**). The complexes were found air stable and soluble in common organic solvents. The proposed structures were formulated on the basis of various spectroscopic techniques *viz.*, IR, NMR (^{1}H, ^{13}C and ^{77}Se) and HR–MS.

Scheme II: Synthesis of Ru(II)–arene complexes **1–4**.

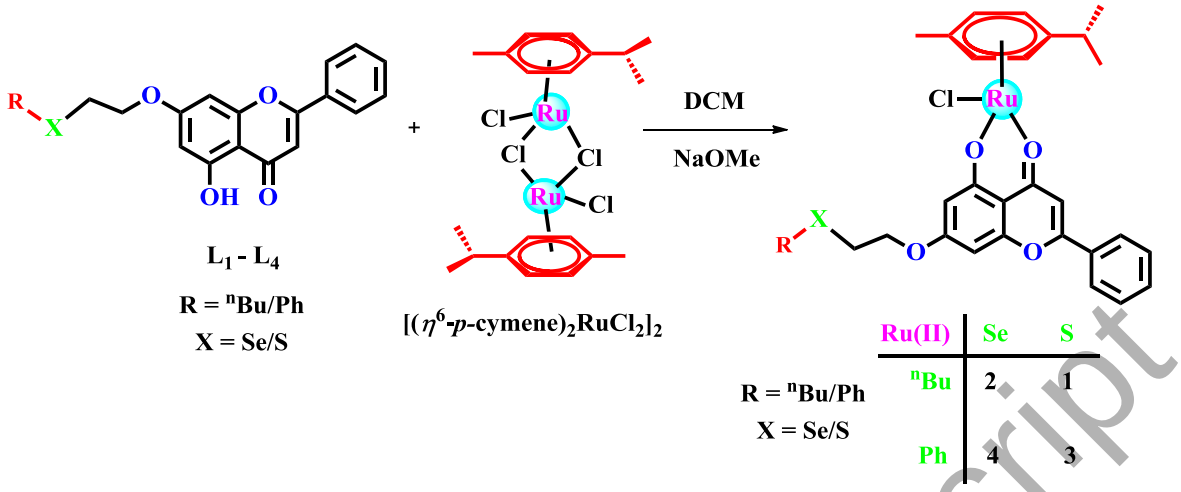

The comparative IR spectra of the ligands, **L_1–L_4** and their corresponding organoruthenium(II) complexes**1–4** provided intricate details about the binding behavior and coordination mode with the metal ion. IR spectra of ligands, **L_1–L_4** exhibited broad band at ~3456 cm^{-1} assigned to hydroxyl –OH group which was found absent in complexes, implicating the coordination of hydroxyl group with the metal ion *via* deprotonation (Raut and Wender, 1959). Another important feature observed in the IR spectra of complexes **1−4** was significant lower frequency shift (~15 cm^{-1}) in the stretching vibrations of ν(C=O), which suggested the chelation of chrysin unit of ligand as a O,O′–bidendate donor to the Ru(II) centre (Pettinari et al., 2005).

The ^{1}H NMR spectra of complexes**1–4** recorded in $CDCl_3$ revealed the absence of –OH signal at ~δ 12.7 ppm indicating the deprotonation of phenolic –OH group on coordination to Ru(II) centre. The spectra of complexes **1–4**, further exhibited two signals as triplet centered at ~δ 4.20 and ~δ 2.90 ppm, corresponding to $OC\underline{H}_2CH_2$ and $OCH_2C\underline{H}_2$, respectively. Additionally, all complexes exhibited signals at ~δ5.54 and ~δ5.26 ppm as doublet, corresponding to protons of *p*–cymene moiety. However, complexes **1** and **2** exhibited multiplet signals in the range of δ 3.28–0.93 ppm assigned to αCH_2, βCH_2, γCH_2 and–CH_3 protons of butylchalcogenide substituent, merged with the characteristic CH_3 and CH protons of *p*–cymene moiety. While, for complexes **3** and **4**the aromatic signatures of the phenylchalcogenide protons were found to be merged in the range of δ 8.82–7.21 ppm (**Fig. S1**).

In^{13}C NMR spectra of the complexes, appreciable downfield shift from 182.4 to 178.1 ppm of C=O carbon was observed as a consequence of the coordination to Ru(II), while the O–C–Ar

carbons of the chrysin appeared in the range ofδ167.73–98.64 ppm. Furthermore, complexes **1–4** displayed signature carbons of *p*–cymene moiety at18.07, 24.08, 30.86, 78.91, 82.33, 90.60 and 97.01 ppm, implicating the coordination of Ru(II)–*p*–cymene fragment. Other peaks corresponding to the $OCH_2\underline{C}H_2$ and $O\underline{C}H_2CH_2$ carbons were also observed at 32.7 and 69.0 ppm, respectively in all the complexes **1–4** (**Fig. S2**).

In order to provide further evidence, ^{77}Se NMR spectra of selenium bearing entities were recorded in $CDCl_3$. The ligands, $\mathbf{L_2}$ and $\mathbf{L_4}$ exhibited a sharp singlet at 144.14 and 271.52 ppm, respectively which shifted marginally to 142.65 and 269.84 ppm in Ru(II) complexes **2** and **4** (**Fig. S3**), excluding any possibility of coordination of organoseleno moiety to Ru(II) metal centre.

HR–MS spectra of the ligands, $\mathbf{L_1}$**–**$\mathbf{L_4}$ displayed prominent peaks at *m/z* 419.06, 439.03, 371.13 and 391.10, respectively corresponding to the $[M+H]^+$ molecular ion fragment (**Fig. S4**) whereas the spectra of Ru^{II} complexes **1–4** were dominated by species assigned to $[M–Cl]^+$ at *m/z* 653.07, 673.03, 605.12 and 625.09, respectively (**Fig. S5**).

The UV–Vis spectra of complexes **1–4** were recorded in DMSO at room temperature exhibited characteristic higher energy intense absorption band in the range of 272–276 nm which could be attributed to the intraligand π→π* transitions. Other low energy broadband in the spectra of complexes observed at 416–475 nm arise from π→π* (MLCT) transitions due to the interaction of filled metal orbitals of low spin d^6 Ru(II) ion with the π* orbitals of the ligand.

3.1. DNA Interaction Studies

Genomic DNA is one of the primary intracellular target (Hosoya and Miyagawa, 2014) for numerous FDA–approved inorganic (cisplatin, carboplatin, oxaliplatin etc.) and organic (doxorubicin, gemcitabine, 5–fluorouracil etc.) chemotherapeutic drugs which exert their anticancer effect by damaging the DNA replication (Kumar, Dasari and Patra, 2017; Tanzadehpanaha et al., 2018). During the past decade, a significant amount of reserch work has been directed on the DNA–binding ability of organometallic Ru(II) complexes (Caruso et al., 2014; Frik et al., 2014) which have indicated differences in mode of DNA interaction depending on their structure. DNA can provide three distinct binding modes for metal complexes viz., intercalation, groove binding and electrostatic binding to phosphate backbone of DNA. Usually, intercalation within the base pairs of DNA results in hypochromism with or without red/blue shift, while non–intercalative, electrostatic interaction with DNA double helix causes

hyperchromism (Liu et al., 2010).The interaction of complexes **1–4** with DNA causes electronic perturbations in these complexes which can be observed by UV–vis absorption, fluorescence and CD spectroscopic studies.

3.1.1. UV–vis absorption studies

The UV–vis spectra of $Ru^{II}(\eta^6$–*p*–cymene)complexes **1–4** exhibited an intense absorption band centered at ~274 nm attributable to π→π* intraligand (IL) transitions. On addition of increasing concentration of CT DNA (0.1–1.0 x 10^{-6}M) to a fixed concentration of complexes **1–4** (0.2 x 10^{-6}M), significant hyperchromism along with blue shifts were observed (**Fig. 2**).

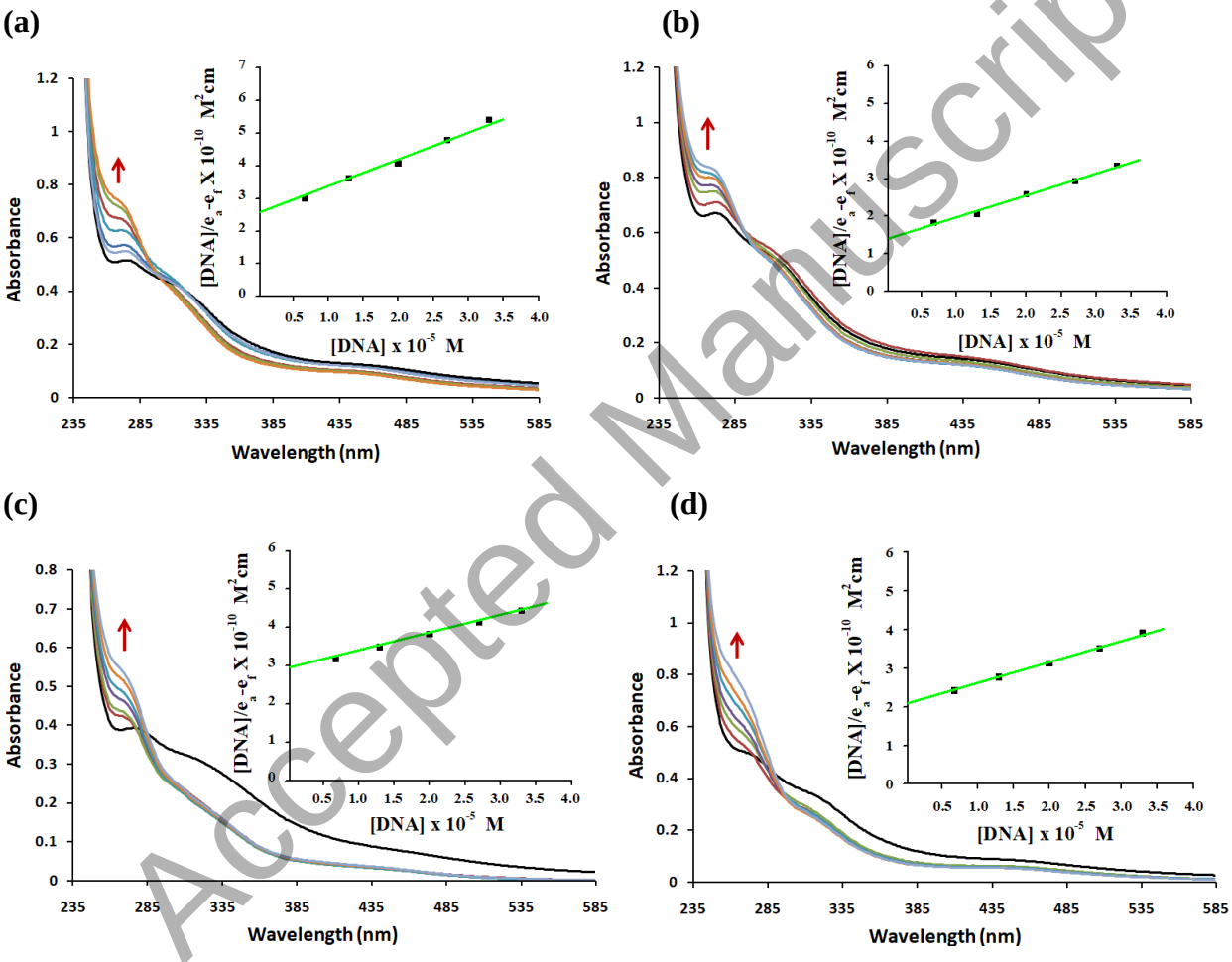

Fig. 2. Absorption spectra of complexes (a) **1**, (b) **2**, (c) **3** and (d) **4** (0.2 x 10^{-6} M) in the presence of increasing concentrations of CT DNA (0.1–1.0 x 10^{-6} M), obtained in Tris–HCl buffer (pH 7.2).

The observed 'hyperchromic effect' along with a blue shift may be attributed to non–covalent interaction preferably *via* external contact due to electrostatic binding to DNA helix (Long and

Barton, 1990; Pasternack, Gibbs and Villafranca, 1983). To quantify the extent of binding of Ru(II) complexes **1–4** to CT DNA, the intrinsic binding constant, K_b values were determined by monitoring the changes in the absorbance at the corresponding λ_{max} with increasing concentrations of CT DNA. Shifting in the position of absorption bands and binding constant, K_b values were calculated from Wolfe–Shimer equation (1), and are summarized in **Table 1**. From the binding constant values it is inferred that, among the chrysin Ru(II) complexes organoseleno– derivatives **2** and **4** exhibited higher binding propensity towards CT DNA in comparison to organothio– derivatives **1** and **3**, following the order **2** > **4** > **1** > **3**, thereby suggesting significant effect of organoselenium moiety on DNA binding interaction. Moreover, efficient binding of butyl derivatives in comparison to their phenyl derivatives is attributed to the increased lipophilicity of the complex due to the presence of aliphatic chain (Batchelor, Paunescu, Soudani, Scopelliti and Dyson, 2017).

Table 1: Binding constant values (K_b) for interaction of complexes **1–4** with DNA.

Complexes	**Absorption λ_{max} (nm)**			**Hyperchromicity (%)**	***K_b* (M^{-1})**
	Free (nm)	**Bound (nm)**	**Δ (nm)**		
1	272	268	4	28	$3.86(\pm0.09) \times 10^5$
2	274	269	5	24	$6.35(\pm0.12) \times 10^5$
3	273	268	5	30	$1.73(\pm0.07) \times 10^5$
4	276	270	6	36	$4.71(\pm0.11) \times 10^5$

3.1.2. Fluorescence spectroscopy

Further insight in the interaction mode of complexes with DNA, fluorescence studies were carried out. The emission spectra of complexes **1–4** displayed an intense luminescence at ~350 nm in Tris–HCl buffer at room temperature in the absence of DNA when excited at 270 nm. The concomitant addition of CT DNA (0–1.2 x 10^{-6} M) to a fixed concentration (0.2 x 10^{-6} M) of complexes **1–4**, resulted a significant enhancement in the fluorescence emission intensity with no apparent change in the shape and position of the emission bands (**Fig. 3**).

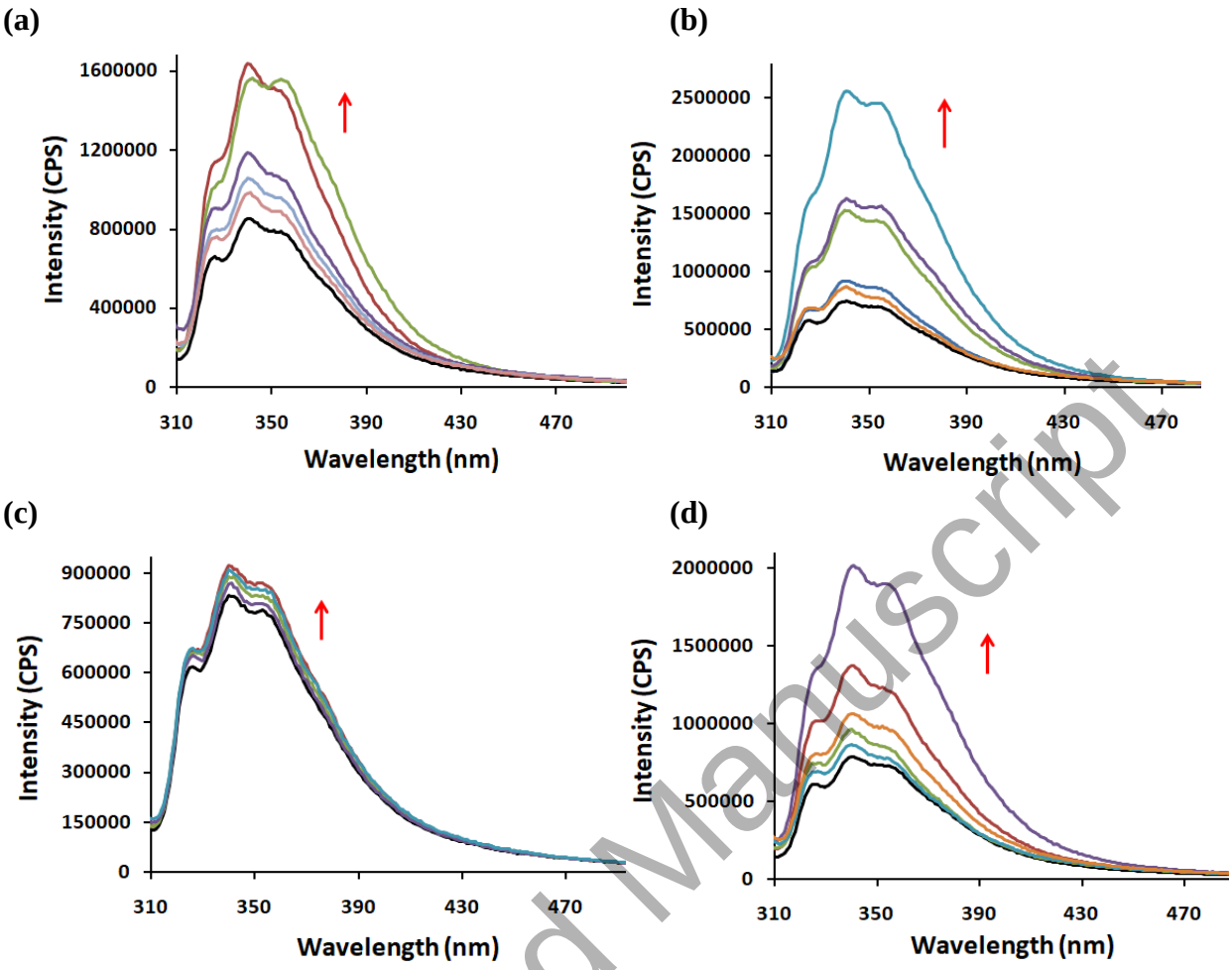

Fig. 3. Fluorescence spectra of complexes (a) **1**, (b) **2**, (c) **3** and (d) **4** (0.2 x10^{-6} M) in the presence of increasing concentrations of CT DNA (0–1.2 x 10^{-6} M) in Tris–HCl buffer (pH 7.2).

The observed enhancement in emission intensity is related to the extent with which that complexes are protected inside the hydrophobic environment of DNA helix. Therefore, the binding of complex to DNA restricts the complex mobility at the binding site due to the inaccessibility of the solvent water molecules, leading to decrease in vibrational mode of relaxation and thus avoiding the quenching effect of solvent molecules. The quantitative assessment of DNA binding strength of the complexes **1–4** was ascertained by binding constant, *K* as quatified by Scatchard equation (2 & 3) and were found to be 4.73 (±0.05) x 10^5, 7.68 (±0.11) x 10^5, 2.04 (±0.07) x 10^5 and 5.81 (±0.15) x 10^5 M^{-1}, respectively, consistent with absorption spectral studies.

3.1.3. Circular dichroism

Circular dichroic (CD) spectroscopy is a powerful technique for monitoring the morphological and conformational transitions in proteins and nucleic acids upon interaction with small molecules. The conformational changes in DNA structure upon interaction with complexes **1–4** was studied by circular dichroism (CD) spectra. The CD spectrum of CT DNA consists of a positive band at 275 nm due to base stacking and a negative band at 245 nm, attributed to right–handed helicity of B–DNA. Simple groove binding and electrostatic interaction of the complexes with DNA showed less or no perturbations on the base stacking and helicity bands, while intercalation can stabilize the helix conformation of B–DNA, and enhance the intensities of both the CD bands (Norden and Tjerneld, 1982). In our experiments, the CD spectra of CT DNA in presence of complexes **1–4** demonstrated decrease in the intensities of both the negative and positive bands without any shift in the band position (**Fig. 4**). These results suggested that the complexes induce distortion of the secondary structure of B–DNA without the alteration in its conformation from B– to A–form or B– to Z–form. However, CD spectral changes clearly ruled out the intercalative mode of binding and demonstrated non–covalent interaction between the complexes and DNA, probably *via* electrostatic mode. Furthermore, the change in intensity followed the order **2** > **4** > **1** > **3**, which were consistent with the results obtained by UV–vis and fluorescence spectroscopy.

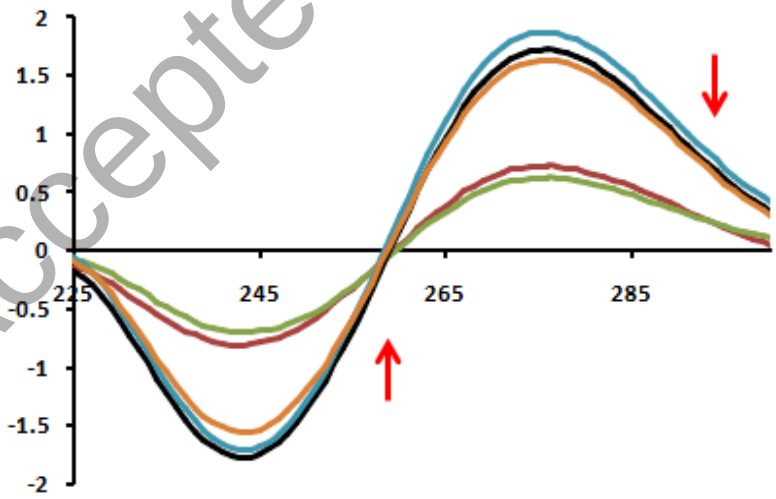

Fig.4. CD spectra of CT DNA alone (blue), CT DNA + **1** (orange), CT DNA + **2** (green), CT DNA + **3** (black) and CT DNA + **4** (red) in Tris–HCl buffer (pH = 7.2). [Complex] = 10^{-6} M, [DNA] = 10^{-6} M.

3.2. HSA Interaction Studies

HSA is identified as the primary transporter of various pharmaceutical drugs particularly following intravenous administration (Sarkar, 1989). It has been reported that interactions of drug entities with HSA most likely involve non–covalent forces which increases their circulatory half–lives in the blood and improves biodistribution throughout the body. Hence, interaction of Ru(II) complexes with serum protein is recognized as an important aspectin determining their pharmacological properties *viz.*, the absorption, transportation, distribution, metabolism, excretion and efficacy of these metal based drugs (Canovic et al., 2017; Karami, Lighvan, Farrokhpour, Jahromi and Momtazi-borojeni, 2017). Keeping in view the immense importance of drug–HSA interaction in the area of pharmacology, the interaction of R(II)–arene complexes with HSA were carried out using UV–vis spectroscopy, fluorescence spectroscopy and circular dichroism (CD) studies.

3.2.1. UV–vis absorption studies

HSA protein exhibited a characteristic absorption peak at~280 nm attributed to aromatic rings in tryptophan (Trp–214) tyrosine (Tyr–411) and phenylalanine (Phe) amino acid residues. A fixed concentration of HSA (2.0 x 10^{-6} M) was titrated with increasing concentration of complexes **1–4**(0–4.0 x 10^{-6} M) (**Fig. 5**). The complexes exhibited hyperchromism at λ_{max}~280 nm along with blue shift, indicating that more aromatic residues were extended into the aqueous environment (Wang et al., 2011). Further, the observed "hyperchromism" suggested the interaction between HSA and complexes due to the formation of ground state complex of the type HSA–Ru(II)complex most likely by electrostatic attraction between the Ru(II) complexes and HSA. Overall, the changes in the absorbance spectra indicated that the microenvironment of the three aromatic residues was altered causing prominent perturbation in tertiary structure of HSA. Meanwhile, binding constant, K_b values for the complexes **1–4** were found to be 3.91(±0.12) x 10^4, 7.23(±0.09) x 10^4, 2.16 (±0.15)x 10^4 and 5.70(±0.07) x 10^4 M^{-1}, respectively suggesting the moderate binding propensity with HSA followed by conformational changes in its structure. Since moderate affinity of a drug towards a protein helps in the diffusion of the drug from the circulatory system to reach its target site, thus obtained K_b values for complexes fulfill this criterion for their transport in the blood circulation and diffusion at the target site. Further, binding affinity of **1–4** falls in the order **2** > **4** > **1** > **3**, which supports that repalcing the phenyl

entity by butyl group at the chalcogen moiety of the chrysin increases the electron donating ability of the substituent which consequently increases the protein binding ability of the complex.

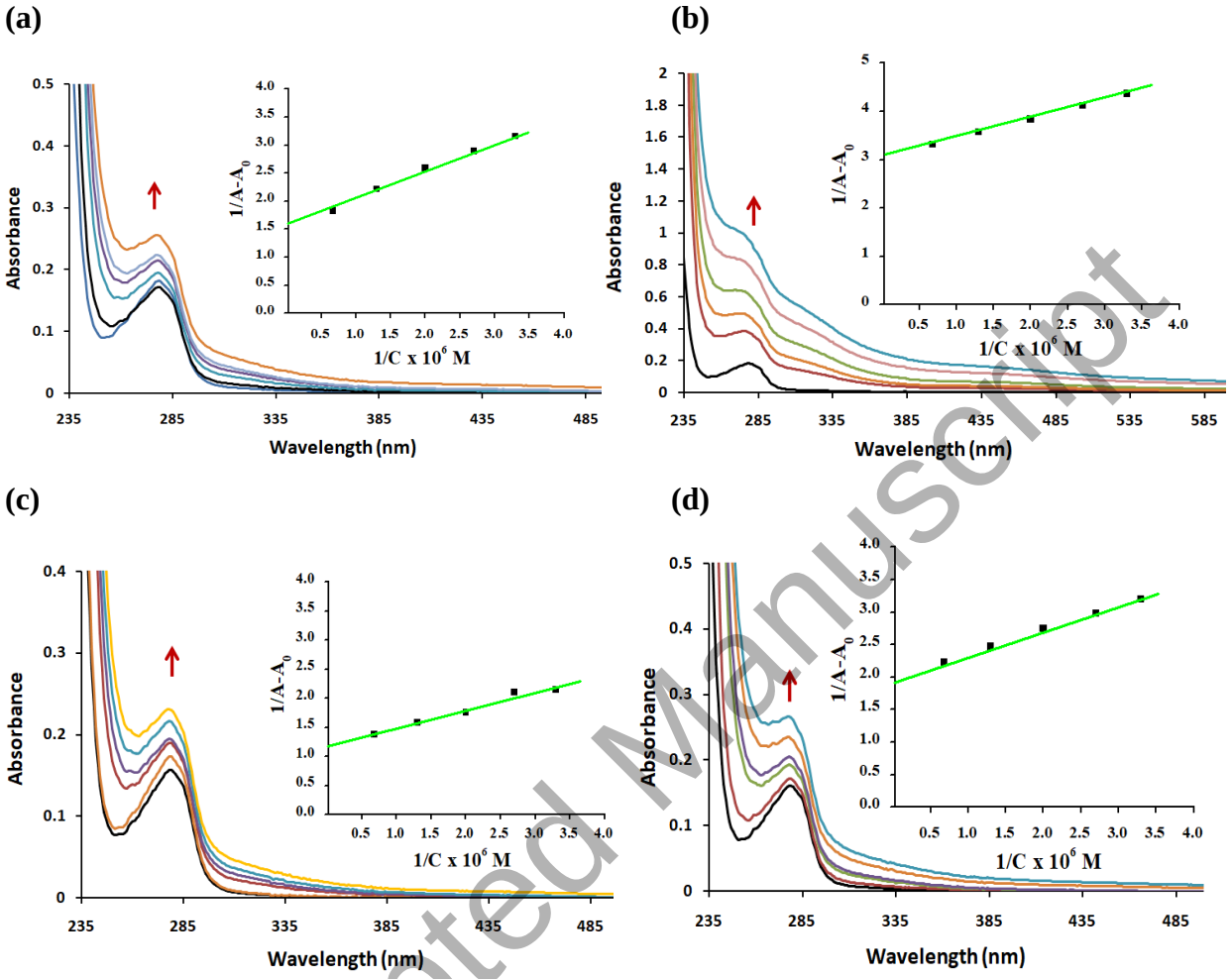

Fig. 5. Absorption spectra of HSA (2.0 x 10^{-6} M) in the presence of increasing concentrations of complexes (a) **1**, (b) **2,** (c) **3** and (d) **4** (0–4.0 x 10^{-6} M) in Tris–HCl buffer (pH 7.2). Arrows indicate the absorbance changes upon increasing concentration of complex.

3.2.2. Fluorescence spectroscopy

HSA is a polypeptide chain with 585 amino acids, of the amino acids single tryptophan residue (Trp–214) is mainly responsible for the majority of the intrinsic fluorescence of the protein. HSA exhibits strong fluorescence emission peak at ~350 nm due to tryptophan residues, when excited at ~290 nm (Lakowicz, 2006) wavelength. Quenching in the fluorescence emission spectra of tryptophan in HSA are primarily due to changes in protein conformation, subunit association,

substrate binding or denaturation. The concomitant addition of $Ru^{II}(\eta^6$–*p*–cymene) complexes **1–4** (0.0–4.0 x 10^{-6} M) to a fixed amount of HSA (1.0 x 10^{-6} M), resulted in quenching of the intrinsic fluorescence intensity of HSA at ~350 nm along with a blue shift of ~3 nm (**Fig. 6**). The observed quenching may be attributed to changes in tryptophan environment of HSA due to the binding of complexes to the albumin, leading to conformational alterations in the tertiary structure of HSA (Rajendiran et al., 2007). **Fig. 7** represents the Stern–Volmer quenching plot of the complexes with HSA.

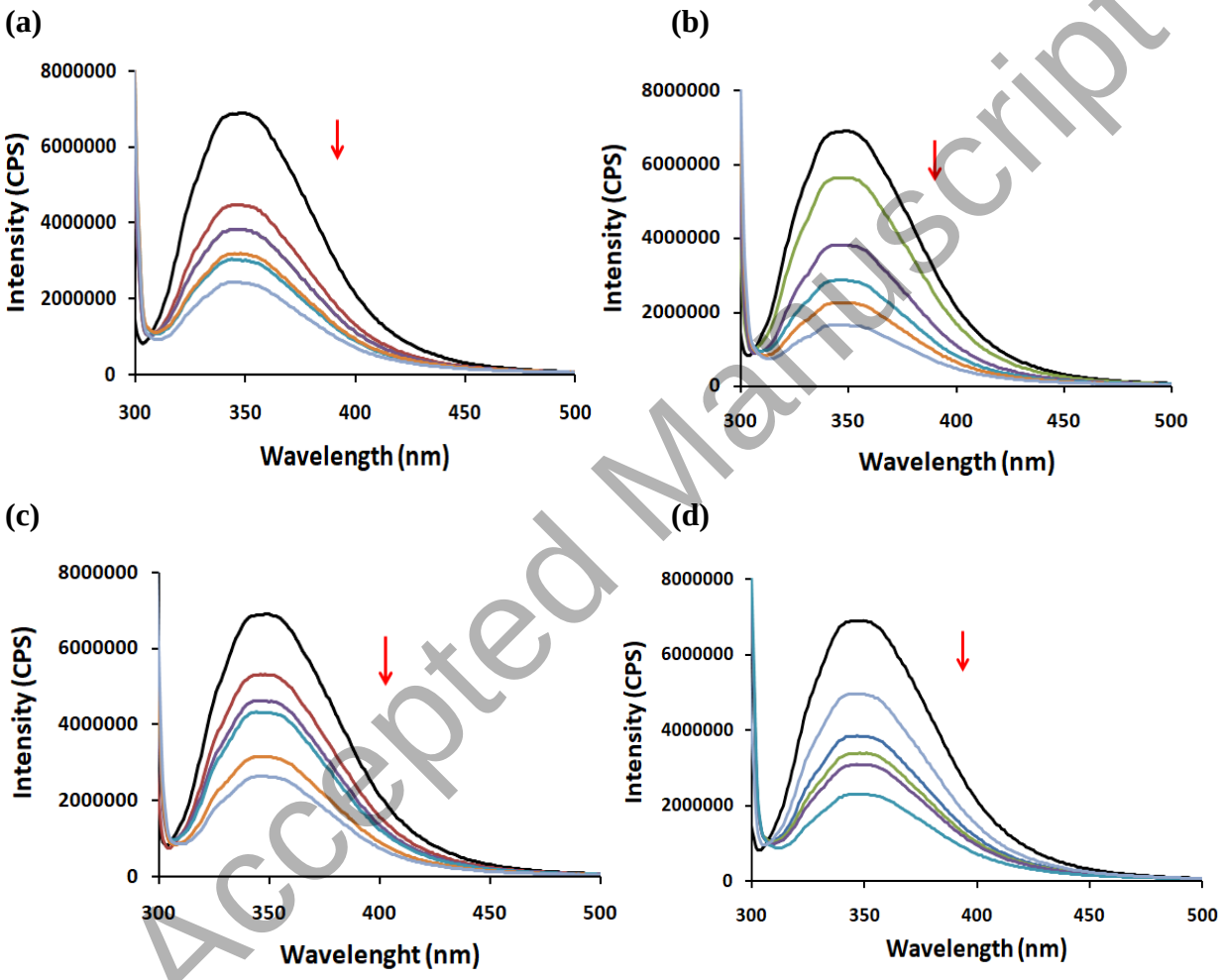

Fig. 6. Fluorescence spectra of HSA (1.0 x 10^{-6} M) in the presence of increasing concentrations of complexes (a) **1**, (b) **2**, (c) **3** and (d) **4** (0–4.0 x 10^{-6} M), obtained in Tris–HCl buffer (pH 7.2) upon excitation at 290 nm.

The quenching can be either *via* static or dynamic mechanism, which was validated by carrying out temperature–dependent fluorescent experiments. Static quenching refers to fluorophore–

quencher complex formation in the ground state, while in dynamic quenching the interaction between fluorophore and quencher is during transient existence of the excited state (Ramachandran, Raja, Bhuvanesh and Natarajan, 2012; Raja, Bhuvanesh and Natarajan, 2011). If the quenching constant (K_{sv}) increased by the increase in temperature then mechanism of quenching is dynamic since at a higher temperature molecules results in rapid diffusion, leading to decrease in collision probability. On the other hand, if K_{sv} decreases by the increase in temperature, then mechanism of quenching is static because the static quenching is caused by the formation of complex and an increase in temperature lowers the stability of the complex and the value of quenching constant.

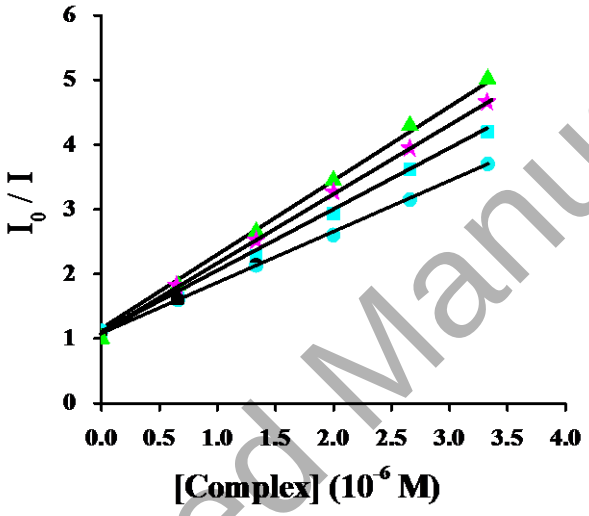

Fig. 7. Stern–Volmer plot for quenching of the complexes **1** (cyan), **2** (green), **3** (red) and **4** (magenta) with HSA.

The fluorescence quenching experiments were performed at two different temperatures *viz.*, 300 and 310 K. As depicted in **Table 2**, an inverse correlation between the Stern–Volmer quenching constant (K_{sv}) values and temperature was noticed. Moreover, the biomolecular quenching rate constant (K_q) values for all Ru(II) complexes were much greater than the maximum value of dynamic quenching (2.0 x 10^{10} mol L^{-1} s^{-1}), suggesting that the fluorescence quenching of HSA was triggered *via*the static quenching mechanismthrough the formation of a complex (Zhao, Liu, Chi, Teng and Qin, 2010). The number of binding sites (n) were calculated ~1, which strongly supported the existence of a unique binding site in HSA for all complexes. Comparing the affinity of complexes **1–4** for HSA, it is inferred that **2** exhibited higher affinity for HSA.

Further, the values of the quenching rate constant (K_q) and binding constant (K) for complexes **1–4** were found to be similar to the values reported for ruthenium(II) complexes (Kljun et al., 2013).

Table 2: Binding and thermodynamic parameters of complex–HSA system at different temperatures obtained from fluorescence quenching experiments (pH 7.2).

Complexes	**T** (K)	K_{sv} (M^{-1})	k_q ($M^{-1}s^{-1}$)	K(M^{-1})	n
1	300	1.93×10^4	1.20×10^{12}	3.90×10^4	0.97
	310	0.73×10^4	0.85×10^{12}	2.07×10^4	
2	300	5.15×10^4	4.45×10^{12}	13.54×10^4	1.34
	310	3.63×10^4	3.89×10^{12}	11.21×10^4	
3	300	1.38×10^4	0.91×10^{12}	1.89×10^4	0.80
	310	0.51×10^4	0.67×10^{12}	0.73×10^4	
4	300	2.74×10^4	3.51×10^{12}	9.68×10^4	1.02
	310	1.99×10^4	2.28×10^{12}	7.53×10^4	

3.2.3. Thermodynamic parameters

The noncovalent interactions with protein are of four types, which are hydrogen–bonding, hydrophobic interaction, van der Waals interaction and ionic interaction (Moradi, Khorasani–Motlagh, Rezvani, and Noroozifar, 2018). The signs and magnitude of thermodynamic parameters *viz.,* change in enthalpy (ΔH), entropy change (ΔS), and free energy change (ΔG), are the main evidence to determine the interaction mode between Ru(II) complexes and HSA. The thermodynamic parameters, $\Delta H > 0$ and $\Delta S > 0$ imply a hydrophobic interaction; $\Delta H < 0$ and $\Delta S < 0$ reflect the van der Waals or hydrogen bond formation and $\Delta H < 0$ and $\Delta S > 0$ suggestive of electrostatic interactions. The calculated thermodynamic parameters are summarized in **Table 3**, showing the negative ΔH and positive ΔS values for the complexes which suggested that the complexes bind to HSA through van der Waals force or hydrogen–bonding. Nevertheless probability of binding of phenyl appended analogs **3** and **4** to HSA *via* hydrophobic interaction cannot be ruled out (Fu et al., 2014). Moreover, all the complexes showed negative values of ΔG,

implicating the spontaneous binding process and the lower ΔG values for **2** supported its higher binding affinity towards HSA.

Table 3: Thermodynamic parameters of complex–HSA interaction at pH 7.2.

Complexes	**T** (K)	**ΔG** (**KJ mol^{-1}**)	**ΔH** (**KJ mol^{-1}K^{-1}**)	**ΔS** (**J mol^{-1}K^{-1}**)
1	300	–23.86	–6.60	57.53
	310	–24.43		
2	300	–29.18	–9.91	64.23
	310	–29.82		
3	300	–21.86	–5.80	53.53
	310	–22.39		
4	300	–26.36	–8.43	59.76
	310	–26.95		

3.2.4. Circular dichroism

CD measurements were performed in the presence of $Ru^{II}(\eta^6$–*p*–cymene) complexes **1–4** to examine its possible impact on the secondary structure of HSA. As depicted in **Fig. 8**, the CD spectrum of HSA revealed two negative bands characteristic of α–helical proteins at 208 and 222 nm assignable to π→π* and n→π* transitions, respectively. The ellipticity of HSA decreased moderately on the addition of complexes, indicating some loss of α–helical secondary structure (Divsalar, Bagheri, Saboury, Mansoori–Torshizi and Amani, 2009). This may imply that complexes could interact with the amino acid residues of the main polypeptide chain of HSA. However, the shape and position of CD spectra remained almost unchanged in presence and absence of complexes, suggesting that conformation of HSA was predominantly in α–helix even after binding to the complexes.

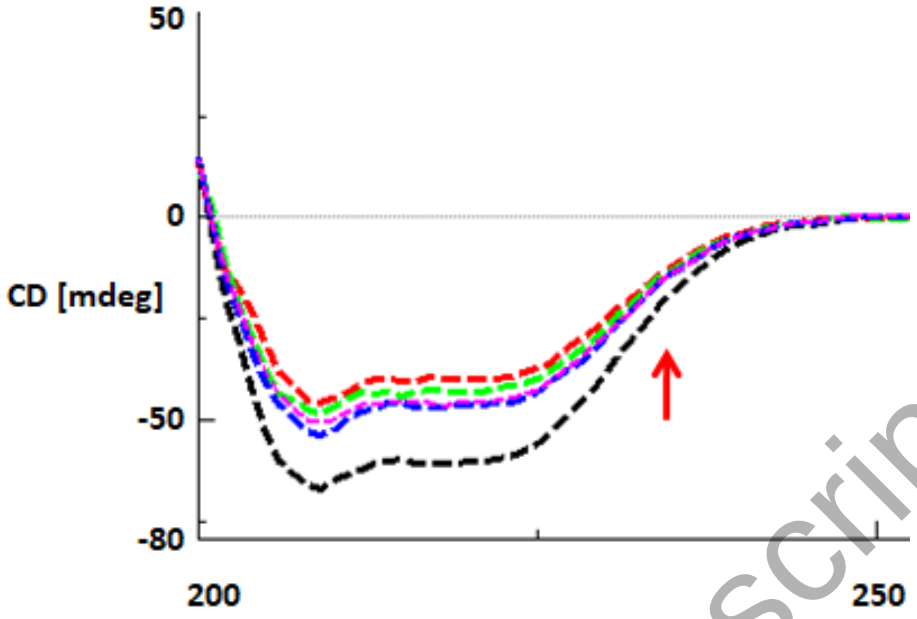

Fig. 8. CD spectra of HSA alone (black), HSA + **1** (pink), HSA + **2** (red), HSA + **3** (blue) and HSA + **4** (green) in Tris–HCl buffer (pH=7.2). [Complex] = 10^{-6} M, [HSA] = 10^{-6} M.

3.2.5. Three–dimensional (3D) fluorescence spectral studies

Three–dimensional (3D) fluorescence spectroscopy is an analytical technique that provides the information about the conformational changes of fluorophore by changing excitation and emission wavelengths simultaneously (Zhang et al., 2008). The presence of **peak *a*** reflects Rayleigh scattering ($\lambda_{ex} = \lambda_{em}$) while **peak *b*** denotes secondary scattering peak ($\lambda_{em} = 2\lambda_{ex}$). **Peak *1*** corresponds mainly to the spectral behavior of Trp and Tyr residues (λ_{ex} ~ 280, λ_{em} ~ 346 nm). Any alteration in the microenvironment of Trp and Tyr residues of HSA upon interaction with complex implicates an obvious change in either intensity or wavelength of the spectra. By comparing the 3D fluorescence spectral changes of HSA in the absence and presence of Ru(II) complexes **1**–**4**, it was observed that the fluorescence intensities of **peak *1*** decreased significantly indicating a strong quenching of fluorescence induced by Trp residue of HSA (**Fig. S6**). However, the quenching phenomena was more pronounced in case of complex **2** indicating its stronger affinity in comparison to other complexes and hence suggested more perturbation in hydrophobic microenvironment near the tryptophan and tyrosine residues leading to conformational changes in HSA.

3.3. Molecular docking studies

3.3.1. Molecular docking with DNA

Molecular docking studies of synthesized $Ru^{II}(\eta^6$–*p*–cymene)complexes **1–4** with DNA duplex of sequence d(CGCGAATTCGCG)$_2$ dodecamer (PDB ID: 1BNA**)** were performed in an attempt to provide vital information regarding the preferred orientation of the complexes inside the DNA grooves. The favorable energy minimized docked poses of *n*–butylseleno complex, **2** revealed that it interact adjacent to AT–rich sequence of the minor groove and was in close proximity to base pairs T7, T8, A18, T19 and T20 of the targeted DNA (**Fig. 9**), while its phenylseleno–analog, **4** showed the interaction in GC–rich region of minor groove adjacent to base pairs C9, G10, C15 and G16 (**Fig. S7**). In general, electronegative AT sequences provide better van der Waals contacts since they are narrower compared to GC regions and therefore expose better fitting for docking of small molecules (Sahoo, Ghosh, Bera and Dasgupta, 2008). Moreover, the stabilization could also be enhanced by extensive van der Waals interaction and hydrophobic contacts in the groove region. Relative binding energy of the docked structures was found to be–278.2, –350.9, –243.6 and –312.1KJ mol^{-1} for**1–4**, respectively, implicating the higher binding affinity of *n*–butylseleno complex **2** as compared to other analogs.

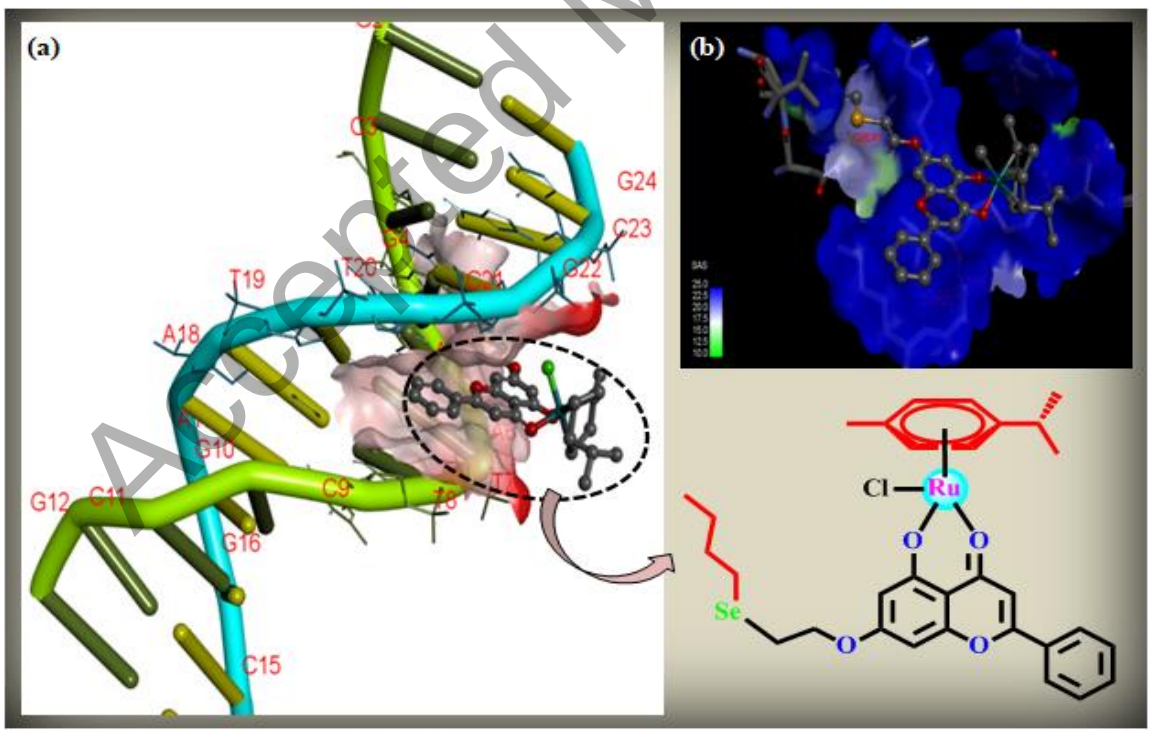

Fig. 9. Molecular docked model of complex **2** in the minor groove of DNA dodecamer duplex of sequence d(CGCGAATTCGCG)$_2$ (PDB ID:1BNA).

3.3.2. Molecular docking with HSA

$Ru^{II}(\eta^6$–*p*–cymene) complexes **1–4** have demonstrated higher binding affinity towards HSA target, and albumins proteins have been identified as the main *in vivo* carrier molecules, so it was imperative to carry out molecular docking studies of $Ru^{II}(\eta^6$–*p*–cymene) complexes with HSA (PDB ID: 1H9Z). Crystal structure descriptions of the 3D structure of HSA revealed a single polypeptide chain of 585 amino acid residues comprises three structurally homologous domains (I–III): I (residues 1–195) II (196–383) and III (384–585); each domain has two subdomains (A and B) that assemble to form heart shaped molecule (He and Carter, 1992; Yamasaki, Chuang, Maruyama and Otagiri, 2013). The principal region of drug binding sites of HSA are located in hydrophobic cavities in subdomain IA and IIA, corresponding to site I and III, respectively and tryptophan residue (Trp–214) of HSA in subdomain IIA. The molecular docking pattern of **2** with HSA indicated that complex was located in the hydrophobic cavity between subdomains IIA and IIIA, implicating the existence of hydrophobic interactions which also results in the fluorescence quenching of Trp–214.

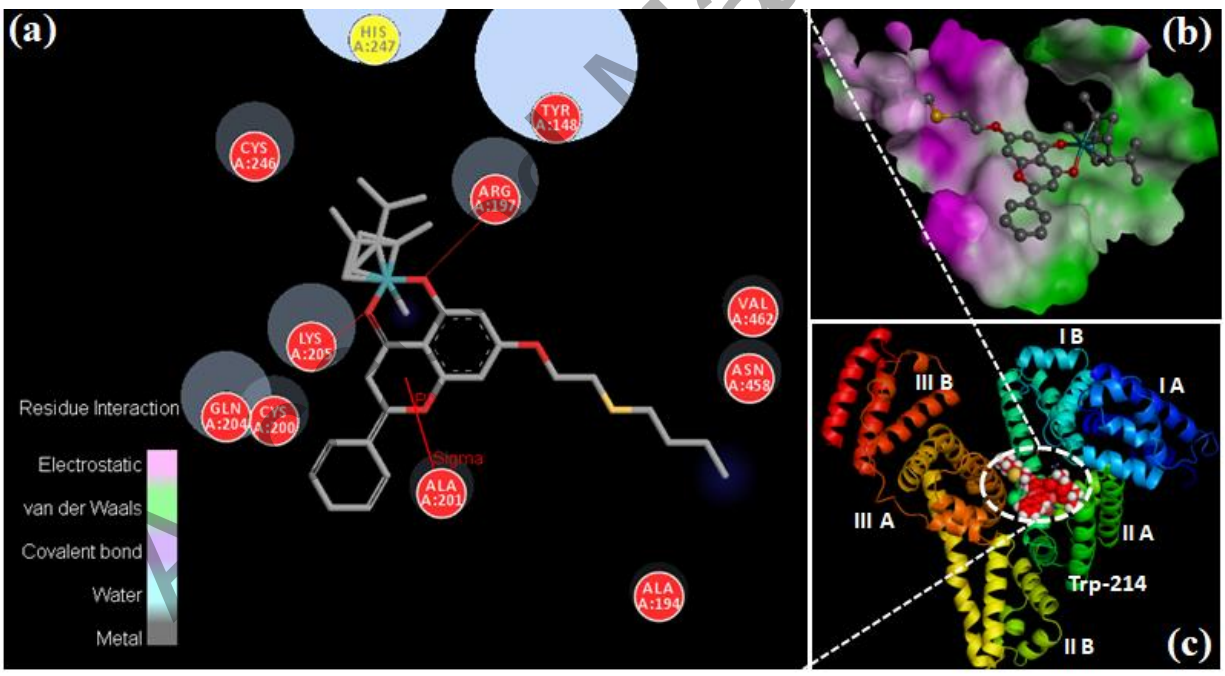

Fig. 10. Molecular docked model of (a) interaction between complex **2** and amino acid residues of HSA (b) complex **2** with HSA and (c) representation of **2** located within the hydrophobic pocket in subdomain III A and II A of HSA.

As clearly depicted in **Fig. 10,** *n*–butylseleno complex **2** was in close proximity of the amino acid residues such as Arg–197, Lys–205, Cys–200, Gln–204, Ala–201, Typ–148, Cys–246, Ala–194, His–247, Asn–458 and Val–462. Our results further revealed that hydrophobic interactions played a major role in **2**–HSA interaction, however hydrogen bonding between Arg–197and Lys–205 residues with O1/2 of O,O– chelating motif of **2** offered additional stability. Further, molecular docking experiments were also performed with phenylseleno derivative, **4** which revealed that complex was found in vicinity of residues *viz*., Lys–162, Ala–158, Lue–155 and Lue–121 (**Fig. 11**). Nevertheless, complex **2** revealed more negative binding energy values towards HSA target than complex **4** thereby showed more binding affinity which correlated well with the *in vitro* binding experiments.

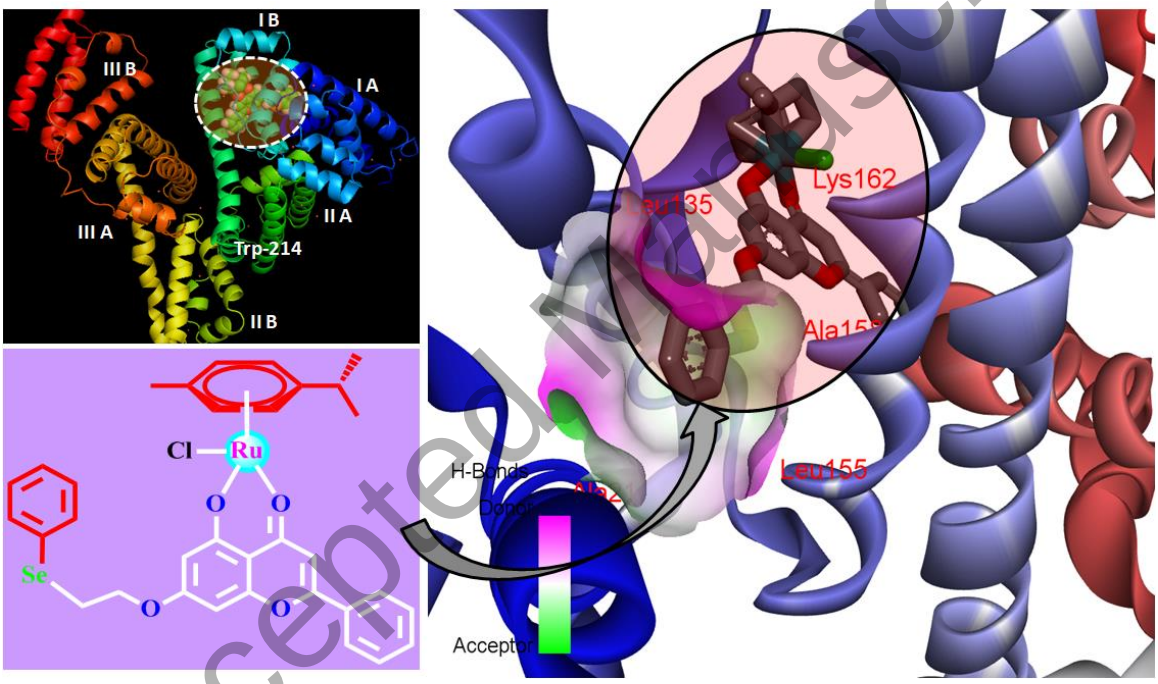

Fig. 11. Molecular docked model of complex **4** with HSA within the hydrophobic pocket in subdomain I B and I A of HSA and its interaction with amino acid residues of HSA.

3.4. In vitro anticancer activity

The cytotoxicity profile of $Ru^{II}(\eta^6$–*p*–cymene) complexes **1–4** were carried out at different molar concentrations in comparison to conventional standard drug Adriamycin (ADR), on selected panel of cancer cell lines *viz.*, HeLa (cervical), MIA–PA–CA–2 (pancreatic), MCF–7 (breast), Hep–G2 (Hepatoma), SK–OV–3 (ovarian) by Sulforhodamine B (SRB) assay. **Fig. 12** shows the

antitumor screening images of different human carcinoma cell lines which demonstrated the good to moderate activity of complexes towards certain specific cancer cell lines.

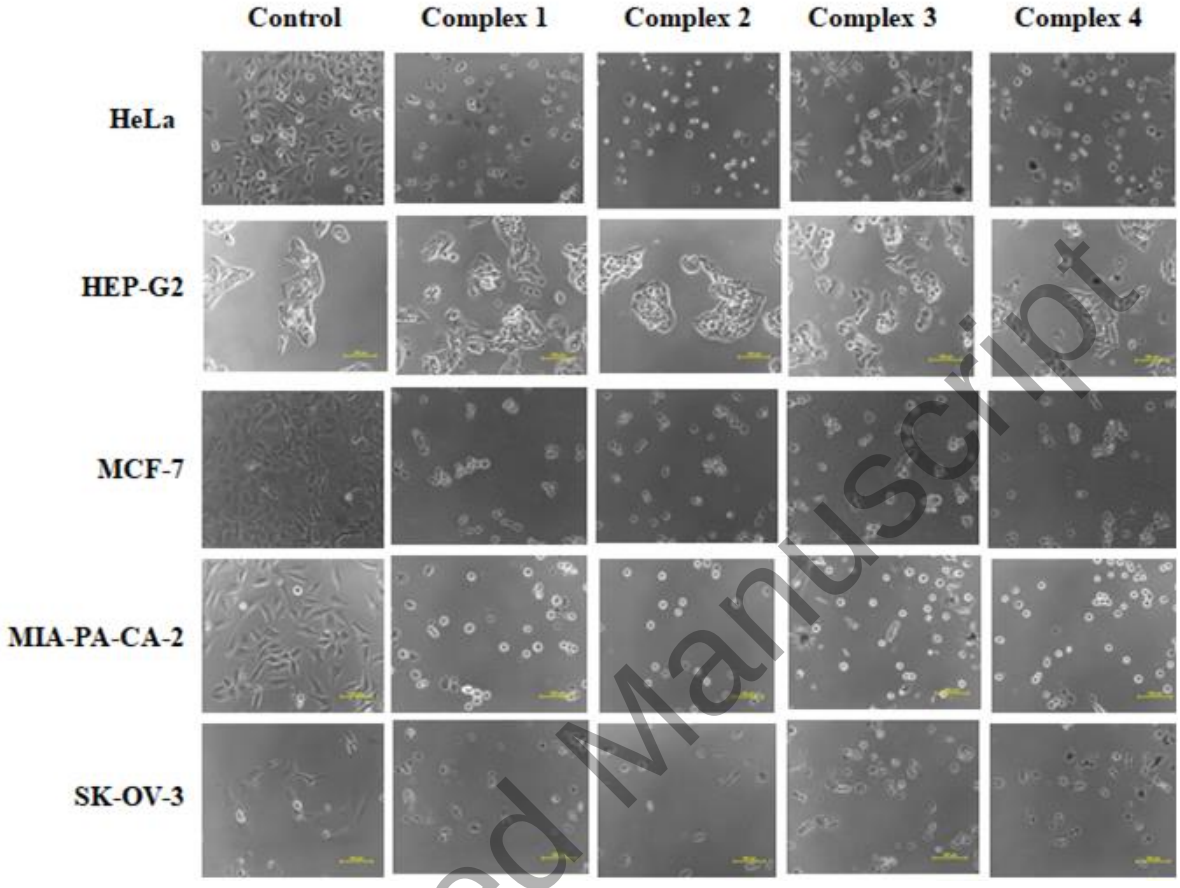

Fig. 12. Images for the *in vitro* cytotoxicity of Ru(II) complexes **1–4** on selected cancer cell lines *viz.*, HeLa (cervical), MIA–PA–CA–2 (pancreatic), MCF–7 (breast), Hep–G2 (Hepatoma), SK–OV–3 (ovarian).

The anticancer screening results showed that all the complexes were effective against HeLa (cervical) cancer cell lines at concentration of 10^{-4} M, although the complexes did not exhibit any detectable cytotoxicity at concentration of 10^{-7} M as compared to Adriamycin. Moreover, ourinitial cytotoxic screening data revealed that complex **2** exhibited comparatively better selectivity and cytotoxicity against certain human cancer phenotypes *viz*., HeLa, MIA–PA–CA–2and MCF–7 at 10^{-4} M which could be presumably due to its higher DNA/HSA binding affinity.

4. Conclusions

Considering the chemotherapeutic effects of chrysin ligand and biological effects of organochalcogen functionalities (S/Se) we have designed hybrid organometallic Ru(II) complexes and explored the influence of these motifs on the anticancer activity as well as on

their modes of action. This work features the design and synthesis of four new $Ru^{II}(\eta^6–p–$cymene) complexes **1–4** derived from organochalcogen (S/Se) functionalized chrysin ligand pharmacophores which were thoroughly characterized by various spectroscopic and analytical techniques. The comparative *in vitro* interaction studies of complexes **1–4**with DNA/HSA targets were carried by employing UV–vis absorption, fluorescence spectroscopy and circular dichroic techniques to validate their chemotherapeutic candidature. Our results demonstrated that $Ru^{II}(\eta^6–p–$cymene) complexes **1–4** exhibited high binding propensity towards CTDNA *via* electrostatic mode and the observed trend in the binding interactions revealed that binding propensity of complexes showed structural dependence *i.e*, seleno– derivatives constitute attractive scaffold and higher binding affinity than their thio– derivatives. Further, mode of interaction of the complexes with DNA/HSA was validated by molecular docking studies, which complemented our spectroscopic observations. The cytotoxicity activity of $Ru^{II}(\eta^6–p–$cymene) complexes **1–4** were carried out by SRB assay against selected human cancer cell lines *viz*., HeLa (cervical), MIA–PA–CA–2 (pancreatic), MCF–7 (breast), Hep–G2 (Hepatoma), SK–OV–3 (ovarian) which demonstrated good activity of all complexes on HeLa cancer cell line, whereas moderate activity on other cell lines, implicating the selective response towards different cancer phenotypes. The results revealed superior cytotoxicity of complex **2** as compared to other complexes on selective cancer phenotypes suggesting that tethering of ^{n}Bu chain over its Ph ring could effectively tune its biological properties.

Supplementary material

Additional supplementary material can be found in the online version of this article.

Acknowledgments

The author S. Yadav thanks Science & Engineering Research Board (SERB) a statutory body of the Department of Science & Technology (DST) for the financial support under project grant PDF/2016/002767. The authors gratefully acknowledge Prof. Yoshiaki Nishibayashi, University of Tokyo, Japan for his valuable inputs in accomplishing this work. The authors are thankful to Department of Chemistry, IIT Delhi for instrumentation facility and Anti–Cancer Drug Screening Facility (ACDSF) at ACTREC, Mumbai for carrying out the *in vitro* anticancer activity.

References

Adhireksan, Z., Davey, G. E., Campomanes, P., Groessl, M., Clavel, C. M., Yu, H., Nazarov, A. A., Yeo, C. H. F., Ang, W. H., Droge, P., Rothlisberger, U., Dyson, P. J., & Davey, C. A. (2014). Ligand substitutions between ruthenium–cymene compounds can control protein versus DNA targeting and anticancer activity. *Nature Communications*, 5, 1–5.

Alessio, E. (2011). *Bioinorganic Medicinal Chemistry*, Wiley–VCH Verlag & Co. KGaA: Weinheim, Germany.

Allardyce, C. S., & Dyson, P. J. (2001). Ruthenium in medicine: Current clinical uses and future prospects. *Platinum Metal Review*, 45 (2), 62–69.

Batchelor, L. K., Paunescu, E., Soudani, M., Scopelliti, R., & Dyson,P. J. (2017). Influence of the linker length on the cytotoxicity of homobinuclear ruthenium(II) and gold(I) complexes. *Inorganic Chemistry*, 56 (16) 9617–9633.

Battin, E. E., & Brumaghim, J. L. (2009). Antioxidant Activity of Sulfur and Selenium: A Review of Reactive Oxygen Species Scavenging, Glutathione Peroxidase, and Metal–Binding Antioxidant Mechanisms. *Cell Biochemistry and Biophysics*, 55, 1–23.

Berndsen, R. H., Weiss, A., Abdul, U. K., Wong, T. J., Meraldi, P., Griffioen, A. W., Dyson, P. J., & Nowak–Sliwinska, P. (2017). Combination of ruthenium (II)–arene complex [Ru(η^6–*p*–cymene)Cl_2(pta)]–(RAPTA–C) and the epidermal growth factor receptor inhibitor erlotinib results in efficient angiostatic and antitumor activity. *Scientific Reports*, 7 (43005) 1–7.

Canovic, P., Simovic, A. R., Radisavljevic, S., Bratsos, I., Demitri, N., Mitrovic, M., Zelen, I., Bugarcic, Z. D., (2017). Impact of aromaticity on anticancer activity of polypyridyl ruthenium(II) complexes: Synthesis, structure, DNA/protein binding, lipophilicity and anticancer activity.*Journal of Biological Inorganic Chemistry*, 22 (7) 1007–1028.

Caruso, F., Monti, E., Matthews, J., Rossi, M., Gariboldi, M. B., Pettinari, C., Pettinari, R., & Marchetti, F. (2014). Synthesis, characterization, and antitumor activity of water–soluble (arene)ruthenium(II) derivatives of 1,3–dimethyl–4–acylpyrazolon–5–ato ligands. First example of Ru(arene)(ligand) antitumor species involving simultaneous Ru–N7(guanine) bonding and ligand intercalation to DNA. *Inorganic Chemistry*, 53 (7) 3668–3677.

Cheng, Li- Y., Fang, M., Bai, A.- M., Ouyang, Y., & Hu, Y. J., (2017). Insights into the interaction of methotrexate and human serum albumin: A spectroscopic and molecular modeling approach. *Luminescence*, 32, 873–879.

Clarke, M. J. (2003). Ruthenium Metallopharmaceuticals. *Coordination Chemistry Reviews*, 236 (1–2), 209–233.

Clavel, C. M., Paunescu, E., Nowak–Sliwinska, P., Griffioen, A. W., Scopelliti, R., & Dyson, P. J. (2015). Modulating the Anticancer Activity of Ruthenium (II)–Arene Complexes. *Journal Medicinal Chemistry*, 58 (8), 3356–3365.

Cui, F., Yan, Y., Zhang, Q., Du, J., Yao, X., Qu, G., & Lu, Y., (2009). Characterization of the interaction between 2′–deoxyuridine and human serum albumin. *Carbohydrate Research*, 344 (5) 642–647.

Cushnie, T. P. T., & Lamb, A. J. (2005). Antimicrobial activity of flavonoids. *International Journal of Antimicrobial Agents*, 26 (5) 343–356.

Divsalar, A., Bagheri, M. J., Saboury, A. A., Mansoori–Torshizi, H., & Amani, M. (2009). Investigation on the interaction of newly designed anticancer pd(ii) complexes with different aliphatic tails and human serum albumin.*Journal of Physical Chemistry B*, 113, 14035−14042.

Dyson, P. J. (2007). Systematic design of a targeted organometallic antitumour drug in pre–clinical development. *Chimia*, 61, 698–703.

Fonseca, S. F., Lima, D. B., Alves, D., Jacob, R. G., Perin, G., Lenardao, E. J., & Savegnago, L., (2015). Synthesis, characterization and antioxidant activity of organoselenium and organotellurium compound derivatives of chrysin. *New Journal of Chemistry*, 39, 3043–3050.

Frik, M., Martinez, A., Elie, B. T., Gonzalo, O., Ramirez deMingo, D., Sanau, M., Sanchez–Delgado, R., Sadhukha, T.; Prabha, S., Ramos, J. W., Marzo, I., & Contel, M. (2014). In vitro and in vivo evaluation ofwater–soluble iminophosphorane ruthenium(II) compounds. A potential chemotherapeutic agent for triple negative breast cancer. *Journal of Medicinal Chemistry*, 57 (23) 9995–10012.

Fu, X.−B., Liu, D.−D., Lin, Y., Hu, W., Mao, Z.−W., & Le, X.−Y. (2014). Water–soluble DNA minor groove binders as potential chemotherapeutic agents: synthesis, characterization, DNA binding and cleavage, antioxidation, cytotoxicity and HSA interactions. *Dalton Trans*actions, 43, 8721−8737.

Grazul, M., & Budzisz, E. (2009). Biological activity of metal ions complexes of chromones, coumarins and flavones. *Coordination Chemistry Reviews*, 253 (21–22) 2588–2598.

Guichard, S. M., Else, R., Reid, E., Zeitlin, B., Aird, R., Muir, M., Dodds, M., Fiebig, H., Sadler, P. J., & Jodrell, D. I. (2006). Anti–tumour activity in non–small cell lung cancer models and toxicity profiles for novel ruthenium(II) based organo–metallic compounds. *Biochemical Pharmacology*, 71 (4) 408–415.

Hall, J. P., Beer, H., Buchner, K., Cardin, D. J., & Cardin, C. J. (2015). The structural effect of methyl substitution on the binding of polypyridyl Ru–dppz complexes to DNA. *Organometallics*, 34, 2481–2486.

Hartinger, C. G., Jakupec, M. A., Zorbas–Seifried, S., Groessl, M., Egger, A., Berger, W., Zorbas, H., Dyson, P. J., & Keppler, B. K. (2008). KP1019, a new redox–active anticancer agent preclinical development and results of a clinical phase I study in tumor patients. *Chemistry & Biodiversity*, 5, 2140–2155.

Hartinger, C. G., Zorbas–Seifried, S., Jakupec, M. A., Kynast, B., Zorbas, H., & Keppler, B. K. (2006). From bench to bedside preclinical and early clinical development of the anticancer agent indazolium trans–[tetrachlorobis(1H–indazole)ruthenate(III)] (KP1019 or FFC14A). *Journal of Inorganic Biochemistry*, 100, 891–904.

He, X. M., & Carter, D. C., (1992). Atomic structure and chemistry of human serum albumin. *Nature*, 358, 209−214.

Hosoya, N., & Miyagawa, K. (2014). Targeting DNA damage response in cancer therapy. *Cancer Science*, 105 (4), 370–388.

Hu, K., Wang, W., Cheng, H., Pan, S., & Ren, J. (2011). Synthesis and cytotoxicity of novel chrysin derivatives. *Medicinal Chemistry Research*, 20 (7) 838–846.

Janakiram, N. B., Mohammed, A., Ravillah, D., Choi, C. I., Zhang, Y., Desai, D., Amin, S., & Rao, C. V., (2013). Chemopreventive effects of PBI–Se, a selenium–containing analog of PBIT, on AOM–induced aberrant crypt foci in F344 rats. *Oncology Reports*, 30, 952–960.

Jaouen, G., & Metzler–Nolte, N., (2010). *Medicinal Organometallic Chemistry*; In Topics in Organometallic Chemistry. Edited by Springer–Verlag, 32.

Jaouen, G., Vessieresab, A., & Top, S. (2015). Ferrocifen type anticancer drugs. *Chemical Society Review*, 44, 8802–8817.

Karami, K., Lighvan, Z. M., Farrokhpour, H., Jahromi M. D., & Momtazi-borojeni, A. A. (2017). Synthesis and spectroscopic characterization study of new palladium complexes containing bioactive O,O-chelated ligands: evaluation of the DNA/protein BSA interaction, in vitro antitumoral activity and molecular docking. *Journal of Biomolecular Structure and Dynamics*, https://doi.org/10.1080/07391102.2017.1391125.

Kelland, L. (2007). The resurgence of platinum–based cancer chemotherapy. *Nature Reviews Cancer*, 7, 573–584.

Kljun, J., Bratsos, I., Alessio, E., Psomas, G., Repnik, U., Butinar, M., Turk, B., & Ture, I., (2013). New Uses for Old Drugs: Attempts to Convert Quinolone Antibacterials into Potential Anticancer Agents Containing Ruthenium. *Inorganic Chemistry*, 52 (15) 9039–9052.

Kubanik, M., Tu, J. K. Y., Sohnel, T., Hejl, M., Jakupec, M. A., Kandioller, W., Keppler, B. K., & Hartinger, C. G. (2015). Expanding on the structural diversity of flavone derived ruthenium II(η^6–arene) anticancer agents. *Metallodrugs*, 1, 24–35.

Kumar, P., Dasari, S., & Patra, A. K. (2017). Ruthenium(II) complexes of saccharin with dipyridoquinoxaline and dipyridophenazine: Structures,biological interactions and photoinduced DNA damage activity. *European Journal of Medicinal Chemistry*, 136, 52–62.

Kurzwernhart, A., Kandioller, W., Bachler, S., Bartel, C., Martic, S., Buczkowska, M., Muhlgassner, G., Jakupec, M. A., Kraatz, H. B., Bednarski, P. J., Arion, V. B., Marko, D., Keppler, B. K., & Hartinger, C. G. (2012). Structure–activity relationships of targeted $Ru^{II}(\eta^6$–*p*–Cymene) anticancer complexes with flavonol–derived ligands. *Journal of Medicinal Chemistry*, 55 (23) 10512–10522.

Kurzwernhart, A., Kandioller, W., Bartel, C., Bachler, S., Trondl, ¨R., Mühlgassner, G., Jakupec, M. A., Arion, V. B., Marko, D., Keppler, B. K., & Hartinger, C. G. (2012). Targeting the DNA–topoisomerase complex in a double–strike approach with a topoisomerase inhibiting moiety and covalent DNA binder. *Chemical Communications*, 48, 4839–4841.

Kurzwernhart, A., Kandioller, W., Enyedy, É. A., Novak, M., Jakupec, M. A., Keppler, B. K., & Hartinger, C. G. (2013). Hydroxyflavones vs. 3–hydroxyquinolinones: structure–activity relationships and stability studies on RuII(arene) anticancer complexes with biologically active ligands, *Dalton Transaction*, 42, 6193–6202.

Lakowicz, J. R. (2006). Principles of Fluorescence Spectroscopy, 3rd ed.; Springer: New York.

Lee, S. S., Park, J. M., Kim, D. Y., Jung, J. H., & Cho, M. H., (1995). Multi–Podands. Ag(I) Complexation with Mono– to Quadru–Podands Having Sulfur Donor. *Chemistry Letters*, 24 (11) 1009–1010.

Liu, Z. C., Wang, B. D., Li, B., Wang, Q., Yang, Z. Y., Li, T. R., Li, Y. (2010). Crystal structures, DNA–binding and cytotoxic activities studies of Cu(II) complexes with 2–oxo–quinoline–3–carbaldehyde Schiff–bases.*European Journal of Medicinal Chemistry*. 45 (11) 5353–5361.

Long, E. C., & Barton, J. K. (1990). On Demonstrating DNA Intercalation.*Accounts of Chemical Research*, 23 (9), 271–273.

Maria G., Ferri, M., Hartinger,C. G., Mendoza, M. A., Groessl,M., Egger,A. E., Eichinger,R. E., Mangrum,J. B., Farrell,N. P., Maruszak,M., Bednarski, P. J., Klein, F., Jakupec, M. A., Nazarov,A. A., Severin, K., &Keppler, B. K. (2009). Transferring the concept of multinuclearity to ruthenium complexes for improvement of anticancer activity. *Journal of Medicinal Chemistry*, 52 (4), 916–925.

Marmur, J. (1961). A procedure for the isolation of deoxyribonucleic acid from micro–organisms. *Journal of Molecular Biology*, 3 (2), 208−218.

Martins, I. L., Miranda, J. P., Oliveira, N. G., Fernandes, A. S., Goncalves, S., & Antunes, A. M., (2013). Synthesis and biological activity of 6–selenocaffeine: potential modulator of chemotherapeutic drugs inbreast cancer cells. *Molecules*, 18, 5251–5264.

Middleton, E., Kandaswami, C., & Theoharides, T. C. (2000). The effects of plant flavonoids on mammalian cells: implications for inflammation, heart disease, and cancer. *Pharmacological Reviews*, 52 (4) 673–751.

Moradi, Z., Khorasani–Motlagh, M., Rezvani, A. R., & Noroozifar,M., (2018). Evaluation of DNA, BSA binding, and antimicrobialactivity of new synthesized neodymium complex containing 29–dimethyl 110–phenanthroline. *Journal of Biomolecular Structure and Dynamics*, 36 (3) 779–794.

Morris, R. E., Aird, R. E., Murdoch, P. d. S., Chen, H., Cummings, J., Hughes, N. D., Parsons, S., Parkin, A., Boyd, G., Jodrell, D. I., & Sadler, P. J. (2001). Inhibition of Cancer Cell Growth by Ruthenium(II) Arene Complexes. *Journal of Medicinal Chemistry*, 44, 3616–3621.

Mustard, D., & Ritchie, D. W., (2005). Docking essential dynamics eigenstructures. *Proteins Proteins: Structure, Function, and Bioinformatics*, 60 (2) 269−274.

Nazarov, A. A., Hartinger, C. G., & Dyson, P. J. (2014). Opening the lid on piano–stool complexes: an account of ruthenium (II)–arene complexes with medicinal applications. *Journal of Organometallic Chemistry*,751, 251–260.

Nguyen, N., Sharma, A., Nguyen, N., Sharma, A. K., Desai, D., Huh, S. J., Amin, S., Meyers, C., & Robertson, G. P., (2011). Melanomachemoprevention in skin reconstructs and mouse xenografts usingisoselenocyanate–4. Cancer Preventive Research, 4, 248–258.

Noffke, A. L., Habtemariam, A., Pizarro, A. M., & Sadler, P. J. (2012). Designing organometallic compounds for catalysis and therapy. *Chemical Communications*, 48 (43), 5219–5246.

Norden, B., & Tjerneld, F. (1982). Structure of methylene blue–DNA complexes studied by linear and circular dichroism spectroscopy. *Biopolymers*, 21 (9) 1713–1734.

Nowak–Sliwinska, P., van Beijnum, J. R., Casini, A., Nazarov, A. A., Wagnieres, G., van den Bergh, H., Dyson, P. J., & Griffioen, A. W. (2011). Organometallic ruthenium(II) arene compounds with antiangiogenic activity. *Journal of Medicinal Chemistry*, 54 (11) 3895–3902.

Pasternack, R. F., Gibbs, E. J., & Villafranca, J. J. (1983). Interactions of porphyrins with nucleic acids.*Biochemistry*, 22 (10), 2406–2414.

Paunescu, E., McArthur, S., Soudani, M., Scopelliti, R., & Dyson, P. J. (2016). Nonsteroidal anti–inflammatory—organometallic anticancer compounds. *Inorganic Chemistry*, 55 (4) 1788–1808.

Pawara, S., Tandela, R., Kunabevub, R., & Jaldappagari, S. (2018). Spectroscopic and computational approaches to unravel the mode of binding between a isoflavone, biochanin-A and calf thymus DNA. *Journal of Biomolecular Structure and Dynamics*, https://doi.org/10.1080/07391102.2018.1442748.

Pettinari, C., Pettinari, R., Fianchini, M., Marchetti, F., Skelton, B. W., & White, A. H., (2005). Syntheses, structures, and reactivity of new pentamethylcyclopentadienyl–rhodium(iii) and –iridium(III) 4–acyl–5–pyrazolonate complexes. *Inorganic Chemistry*, 44 (22), 7933–7942.

Pichichero, E., Cicconi, R., Mattei, M., & Canini, A., (2011). Chrysin induced apoptosis is mediated through p38 and Bax activation in B16–F1 and A375 melanoma cells. *International Journal of Oncology*, 38, 473–483.

Qi, Y., Fu, X., Xiong, Z., Zhang, H., Hill, S. M., Rowan, B. G. & Dong, Y., (2012). Methylseleninic acid enhances paclitaxel efficacy for thetreatment of triple–negative breast cancer. *PLoS One*, 7, e31539.

Rademaker–Lakhai, J. M., Van Den Bongard, D., Pluim, D., Beijnen, J. H., & Schellens, J. H. M. (2004). A phase I and pharmacological study with imidazolium–trans–DMSO–imidazole–tetrachlororuthenate, a novel ruthenium anticancer agent. *Clinical Cancer Research*, 10, 3717–3727.

Rahmanto, A. S., & Davies, M. J. (2012). Selenium–containing amino acids as direct and indirect antioxidants. International Union of Biochemistry and Molecular Biology Life. 64, 863–871.

Raja, D. S., Bhuvanesh, N. S. P., & Natarajan, K. (2011). Biological evaluation of a novel water soluble sulphur bridged binuclear copper(II) thiosemicarbazone complex. *European Journal of Medicinal Chemistry*, 46 (9) 4584–4594.

Rajendiran, V., Karthik, R., Palaniandavar, M., Stoeckli–Evans, H., Periasamy, V. S., Akbarsha, M. A., Srinag, B. S., & Krishnamurthy, H. (2007). Mixed–Ligand Copper(II)–phenolate Complexes: Effect of Coligand on Enhanced DNA and Protein Binding, DNA Cleavage, and Anticancer Activity.*Inorganic Chemistry*, 46 (20) 8208–8221.

Ramachandran, E., Raja, D. S., Bhuvanesh, N. S. P., & Natarajan, K. (2012). Mixed ligand palladium(II) complexes of 6–methoxy–2–oxo–1,2–dihydroquinoline–3–carbaldehyde 4*N*–substituted thiosemicarbazones with triphenylphosphine co–ligand: Synthesis, crystal structure and biological properties. *Dalton Transactions*, 41, 13308–13323.

Raut, K. B., & Wender, S. H., (1959). Synthesis of certain chalcones and 3–hydroxychromones. *Journal of Organic Chemistry*, 25, 50–52.

Reedijk J., (1996). Improved understanding in platinium antitumour chemistry. *Chemical Communications*, 801–806.

Rehman, M. U., Tahir, M., Khan, A. Q., Khan, R., Lateef, A., Oday–O–Hamiza, Qamar, W., Ali, F. & Sultana, S., (2013). Chrysin suppresses renal carcinogenesis via amelioration of hyperproliferation, oxidative stress and inflammation: plausible role of NF–κB. *Toxicology Letters*, 216, 146–158.

Riedl, C. A., Flocke, L. S., Hejl, M., Roller, A., Klose, M. H., Jakupec, M. A.; Kandioller, W., & Keppler, B. K. (2017). Introducing the 4–phenyl–1,2,3–triazole moiety as a versatile scaffold for the development of cytotoxic ruthenium(II) and osmium(II) arene cyclometalates. *Inorganic Chemistry*, 56 (1) 528–541.

Sahoo, B. K., Ghosh, K. S., Bera, R., & Dasgupta, S., (2008). Studies on the interaction of diacetylcurcumin with calf thymus–DNA. *Chemical Physics*, 315 (1–3) 163–169.

Samari, F., Hemmateenejad, B., Shamsipur, M., Rashidi, M., & Samouei, H. (2012). Affinity of Two Novel Five–Coordinated Anticancer Pt(II) Complexes to Human and Bovine Serum Albumins: A Spectroscopic Approach. *Inorganic Chemistry*, 51, 3454−3464.

Sanmartín, C., Plano, D., & Palop, J. A., (2008). Selenium compounds and apoptotic modulation: a new perspective in cancer therapy. *Mini Reviews in Medicinal Chemistry*, 8, 1020–1031.

Sanmartin, C., Plano, D., Sharma, A. K., & Palop, J. A. (2012). Selenium compounds, apoptosis and other types of cell death: an overview for cancer therapy. *International Journal of Molecular Sciences*, 13, 9649–9672

Sarkar, B. (1989). Metal–protein interactions in transport, accumulation, and excretion of metals. *Biological Trace Element Research*, 21 (1) 137–144.

Singh, M., Kaur, M., &Silakari, O., (2014). Flavones: An important scaffold for medicinal chemistry. *European Journal of Medicinal Chemistry*, 84, 206–239.

Smith, G. S., & Therrien, B. (2011). Targeted and multifunctional arene ruthenium chemotherapeutics. *Dalton Transaction*, 40, 10793–10800.

Soares, S., Mateus, N., & de Freitas, V. (2007). Interaction of different polyphenols with bovine serum albumin (BSA) and human salivary α–amylase (HSA) by fluorescence quenching. *Journal of Agricultural and Food Chemistry*, 55 (16), 6726–6735.

Stephanos, J. J. (1996). Drug–protein interactions: Two–site binding of heterocyclic ligands to a monomeric hemoglobin. *Journal of Inorganic Biochem*istry, 62 (3) 155–169.

Tanzadehpanaha, H., Mahakib, H., Moghadamc, N. H., Salehzadehc, S., Rajabid, O., Najafia, R., Aminia R., & Saidijam M., (2018). Binding site identification of anticancer drug gefitinib to HSA and DNA in the presence of five different probes. *Journal of Biomolecular Structure and Dynamics*, https://doi.org/10.1080/07391102.2018.1441073.

Wang, F., Habtemariam, A., van der Geer, E. P., Fernandez, R., Melchart, M., Deeth, R. J., Aird, R., Guichard, S., Fabbiani, F. P., Lozano–Casal, P., Oswald, D. H., Jodrell, D. I., Parsons, S., & Sadler, P. J. (2005). Controlling ligand substitution reactions of organometallic complexes: Tuning cancer cell cytotoxicity.*Proceedings of the National Academy of Sciences of the United States of America*, 102 (51) 18269–18274.

Wang, Y., Wang, X., Wang, J., Zhao, Y., He, W., & Guo, Z. (2011). Noncovalent Interactions between a Trinuclear Monofunctional Platinum Complex and Human Serum Albumin. Inorganic Chemistry, 50 (24) 12661–1266.

Weiss, A., Berndsen, R. H., Dubois, M., Müller, C., Schibli, R., Griffioen, A. W., Dyson, P. J., & Nowak–Sliwinska, P. (2014). *In vivo* anti–tumor activity of the organometallic ruthenium (II)–arene complex [Ru(η^6–*p*–cymene)Cl_2(pta)](RAPTA–C) in human ovarian and colorectal carcinomas. *Chemical Science*, 5 (12), 4742–4748.

Weiss, A., Ding, X., van Beijnum, J. R., Wong, I., Wong, T. J., Berndsen, R. H., Dormond, O., Dallinga, M., Shen, L., Schlingemann, R. O., Pili, R., Ho, C. M., Dyson, P. J., van den Bergh, H., Griffioen, A. W., &Nowak–Sliwinska, P. (2015). Rapid optimization of drug combinations for the optimal angiostatic treatment of cancer. *Angiogenesis*, 18 (3), 233–244.

Wheate, N. J., Walker, S., Craig, G. E., & Oun, R., (2010). The status of platinum anticancer drugs in the clinic and in clinical trials. *Dalton Transactions*, 39 (35), 8113–8127.

Wolfe, A., Shimer G. H., & Meehan, T., (1987). Polycyclic aromatic hydrocarbons physically intercalate into duplex regions of denatured DNA. *Biochemistry*, 26 (20), 6392−6396.

Yamasaki, K., Chuang, V. T. G., Maruyama, T., & Otagiri, M., (2013). Albumin–drug interaction and its clinical implication.*Biochimica et Biophysica Acta*, 1830 (12) 5435−5443.

Yang, B., Huang, J., Xiang, T., Yin, X., Luo, X., Huang, J., Luo, F., Li, H., Li, H., & Ren, G., (2014). Chrysin inhibits metastatic potential ofhuman triple–negative breast cancer cells by modulating matrix metalloproteinase–10, epithelial to mesenchymal transition, and PI3K/Akt signaling pathway. *Journal of Applied Toxicology*, 34, 105–112.

Zeng, H., Cheng, W. H. & Johnson, L. K., (2013). Methylselenol, aselenium metabolite, modulates p53 pathway and inhibits the growthof colon cancer xenografts in Balb/c mice. *Journal of Nutritional Biochemistry*, 24, 776–780.

Zhang, Y.–Z., Chen, X. –X., Dai, J., Zhang, X. –P., Liu, Y. –X., & Liu, Y., (2008). Spectroscopic studies on the interaction of lanthanum(III) 2- oxo- propionic acid salicyloyl hydrazone complex with bovine serum albumin. *Luminescence*, 23, 150−156.

Zhao, X., Liu, R., Chi, Z., Teng, Y.; & Qin, P., (2010). New insights into the behavior of bovine serum albumin adsorbed onto carbon nanotubes: Comprehensive Spectroscopic studies. *Journal of Physical Chemistry B*, 114 (16) 5625–5631.

Research Highlights

- Synthesis and characterization of organochalcogen based chrysin $Ru^{II}(\eta^6–p–$cymene) complexes
- *In vitro* interaction studies of Ru(II) complexes with CT DNA revealed electrostatic mode of interactions with DNA
- The fluorescence studies revealed efficiently quenching of intrinsic fluorescence of HSA *via* a static quenching mechanism.
- Molecular modelling studies correlated with the *in vitro* DNA/HSA binding results.
- SRB assay exhibited superior cytotoxicity of *n*-butylseleno complex on selective cancer phenotypes